Key Points:

- Marine and mineral dust aerosol contributed to ice nucleating particle populations measured from ship and aircraft over the Southern Ocean
- The model predicts observed latitudinal variability in aerosol surface area concentrations at high southern latitudes
- Model-predicted mineral dust ice nucleating particle number concentrations vary by 4 orders of magnitude over the Southern Ocean

Correspondence to:
C. S. McCluskey,
cmcclus@ucar.edu
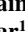
Simulating Southern Ocean Aerosol and Ice Nucleating Particles in the Community Earth System Model Version 2

Christina S. McCluskey[1], Andrew Gettelman[1,2], Charles G. Bardeen[3], Paul J. DeMott[4], Kathryn A. Moore[4], Sonia M. Kreidenweis[4], Thomas C. J. Hill[4], Kevin R. Barry[4], Cynthia H. Twohy[5], Darin W. Toohey[6], Bryan Rainwater[6,7], Jorgen B. Jensen[8], John M. Reeves[8], Simon P. Alexander[9,10], and Greg M. McFarquhar[11,12]

[1]Climate Global Dynamics Laboratory, NCAR, Boulder, CO, USA, [2]Now at Atmospheric Sciences and Global Change, Pacific Northwest National Laboratory, Richmond, WA, USA, [3]Atmospheric Chemistry Observations and Modeling Laboratory, NCAR, Boulder, CO, USA, [4]Department of Atmospheric Science, Colorado State University, Fort Collins, CO, USA, [5]NorthWest Research Associates, Redmond, WA, USA, [6]Department of Atmospheric and Oceanic Sciences, University of Colorado Boulder, Boulder, CO, USA, [7]Now at Handix Scientific Inc, Boulder, CO, USA, [8]Earth Observing Laboratory, NCAR, Boulder, CO, USA, [9]Australian Antarctic Division, Kingston, TAS, Australia, [10]Australian Antarctic Program Partnership, Institute for Marine and Antarctic Studies, University of Tasmania, Hobart, TAS, Australia, [11]Cooperative Institute for Severe and High Impact Weather Research and Operations, Norman, OK, USA, [12]School of Meteorology, University of Oklahoma, Norman, OK, USA

Abstract Southern Ocean (SO) low-level mixed phase clouds have been a long-standing challenge for Earth system models to accurately represent. While improvements to the Community Earth System Model version 2 (CESM2) resulted in increased supercooled liquid in SO clouds and improved model radiative biases, simulated SO clouds in CESM2 now contain too little ice. Previous observational studies have indicated that marine particles are major contributor to SO low-level cloud heterogeneous ice nucleation, a process that initiates a number of cloud processes that govern cloud radiative properties. In this study, we utilize detailed aerosol and ice nucleating particle (INP) measurements from two recent measurement campaigns to assess simulated aerosol abundance, number size distributions, and composition and INP parameterizations for use in CESM2. Our results indicate that CESM2 has a positive bias in simulated surface-level total aerosol surface area at latitudes north of 58°S. Measured INP populations were dominated by marine INPs and we present evidence of refractory INPs present over the SO assumed here to be mineral dust INPs. Results highlight a critical need to assess simulated mineral dust number and size distributions in CESM2 in order to adequately represent SO INP populations and their response to long-term changes in atmospheric transport patterns and land use change. We also discuss important cautions and limitations in applying a commonly used mineral dust INP parameterization to remote regions like the pristine SO.

Plain Language Summary Clouds over the Southern Ocean play an important role in our climate by reflecting significant amounts of solar radiation that would otherwise be absorbed by the ocean. Earth system models used to simulate climate struggle to accurately represent Southern Ocean clouds, largely because there have been limited observations to evaluate and improve models. One specific process that may be important for modeling Southern Ocean clouds is ice nucleation, where ice nucleation active particles serve as "seeds" for ice formation in clouds. In this study, we use measurements from two recent field campaigns to test a state-of-the-art Earth system model's representation of atmospheric particles. We also test three different methods for representing the concentrations of available ice nucleating particles. The results from this work highlight a need for increased knowledge of the quantities, sizes and altitudes of mineral dust particles transported from distant land sources to the Southern Ocean and also emphasizes that Earth system models need to include ice nucleation from marine particles in order to accurately represent aerosol-cloud-climate interactions in these remote regions.

1. Introduction

The Southern Ocean (SO) is one of the cloudiest regions on Earth (Huang et al., 2015; Mace & Protat, 2018) with vast low-level mixed phase clouds that reflect solar radiation. Southern Ocean clouds are an important component of the Earth's energy balance, yet they are challenging to simulate in global climate models. Many Coupled Model Intercomparison Project Phase 5 (CMIP5) models featured too few SO clouds that were over-glaciated,

which resulted in large positive shortwave radiation biases (Bodas-Salcedo et al., 2016). The NCAR Community Earth System Model (CESM) version 1 model included this SO shortwave radiation bias (Kay et al., 2016) and, in company with other CMIP6 models, CESM version 2 (CESM2) included modified model physics that resulted in increased supercooled liquid water over the SO region and reduced shortwave radiation bias (Gettelman et al., 2020).

Many CMIP6 models are associated with significantly higher equilibrium climate sensitivities (ECS) compared to CMIP5, which has been attributed to stronger positive cloud feedbacks in extratropical regions, including the SO region, in CMIP6 models compared to CMIP5 models (Zelinka et al., 2020). Modeling studies have also indicated that the cloud phase feedback over the SO, where ice-containing clouds warm and become liquid-dominated clouds, is important for estimating future climate and ECS (Bjordal et al., 2020; Gettelman, Hannay, et al., 2019; Tan et al., 2016). While simulated low-level cloud phase has improved from CMIP5 to CMIP6, an assessment of CESM2 against aircraft cloud observations demonstrated good agreement with observed liquid water content, but also highlighted a low bias in ice water content, suggesting simulated SO low-level clouds contained too little ice phase and too little total cloud water in CESM2 (Gettelman et al., 2020). These results motivate careful consideration of how models represent processes that influence cloud phase, including heterogeneous ice nucleation.

Heterogeneous immersion freezing is the process by which ice nucleation active particles initiate freezing of supercooled liquid droplets. Ice nucleating particles (INPs) active across the mixed phase temperature range (0 to −38°C) are associated with many aerosol types, including mineral dust, bacteria, biomass burning, and agricultural soils (Kanji et al., 2017). Sea spray aerosol (SSA), comprised of both biogenic organic material and sea salts (O'Dowd et al., 2004), is also a source of INPs (P. J. DeMott et al., 2016). The ice nucleation ability of SSA is linked to ocean biological activity (McCluskey et al., 2017) and multiple INP types are likely associated with SSA. Studies have identified (a) an organic molecular marine INP type that coats sea salt particles and (b) a marine organic microbial INP type that is heat-labile and active at temperatures greater than −20°C (McCluskey, Hill, Sultana, et al., 2018). While marine biogenic INPs may be dominant in southern high latitudes, the IN ability of SSA per surface area of aerosol is up to three orders of magnitude weaker than that of mineral dust aerosol (P. J. DeMott et al., 2016). As such, it is expected that transported land-derived aerosol may significantly influence INP populations in remote polar regions. Ship-based measurements have confirmed that INPs present in the SO marine boundary layer are extremely sparse and are dominated by marine sources (McCluskey, Hill, Humphries, et al., 2018). While modeling studies also indicate marine INPs significantly contribute to the SO marine boundary layer INP population, simulated aerosol vertical profiles suggest that transported mineral dust INPs may out-compete marine INPs at higher altitudes (McCluskey et al., 2019; Vergara-Temprado et al., 2017). Accurately representing the aerosol influence on cloud ice formation relies on increasing our understanding of the aerosol sources and their control on the spatial distribution of SO INP populations, in addition to representing these INPs in models (Vignon et al., 2021).

Many CMIP models, including the CESM, have historically used the Meyers et al. (1992) empirical IN parameterization based on temperature and supersaturation and the Bigg (1953) droplet immersion freezing parameterization. These ice nucleation approaches do not consider aerosol amount or type, and the observations used to develop these schemes did not include remote regions now known to have low INP number concentrations. As such, these parameterizations likely overestimate IN in regions like the SO (e.g., Listowski & Lachlan-Cope, 2017). Ice nucleation was one of the changes made to CESM2 with the implementation of an aerosol-aware classical nucleation theory (CNT) approach to better represent IN (Wang et al., 2014). This new CNT approach predicts mixed-phase immersion freezing rates based on temperature, supersaturation, and the amount of simulated mineral dust aerosol (Wang et al., 2014) and unlike previously used IN schemes, the CNT approach represents regional variability in ice nucleation rates. However, there is a lack of ice nucleation rate observations and it is therefore challenging to evaluate the skill of simulated ice nucleation in CESM2.

In this study, we employ and evaluate a deterministic, rather than stochastic, approach for ice nucleation in CESM2, similar to Zhao et al. (2021). That is, IN is determined based on predicted INP number concentrations using aerosol type-specific deterministic IN parameterizations. We evaluate the amount and types of both aerosol and INP populations in order to identify biases specific to simulating aerosol versus biases specific to INP parameterizations. We describe the methods, models and data in Section 2. Detailed SO aerosol and INP observations from the 2017–2018 Measurements of Aerosols, Radiation and Clouds over the Southern Ocean (MARCUS) and 2018 Southern Ocean Cloud Radiation and Aerosol Transport Experimental Study (SOCRATES)

Table 1
Aerosol and INP Measurements Used From the MARCUS and SOCRATES Campaigns

Variable	Description	Instrument	Size range (dry D_p)	Sampling frequency
N_{UHSAS}	Number concentration of accumulation mode aerosol, #/cm³	UHSAS, SOCRATES	0.07–1.0 µm	1 Hz, 30 s running mean
N_{GNI}	Number concentration of coarse mode sea salt, cm⁻³	GNI, SOCRATES	1.4–32 µm	10 s
S_{tot}	Aerosol surface area, µm² cm⁻³	Nephelometer, MARCUS	<10 µm or <1 µm	5 min
f_x	Number fraction of particles identified as species x	Particle collection & analysis, SOCRATES	0.1–0.5 µm or 0.5–5 µm	10 s
N_{INPs}	Number concentration of ice nucleating particles, L⁻¹	IS, MARCUS	Total suspended aerosol	23–51 hr
N_{INPs}	Number concentration of ice nucleating particles, L⁻¹	IS, SOCRATES	0.2–4 µm	Above and below cloud sampling (10–20 min)

campaigns (McFarquhar et al., 2021) are used to (a) evaluate simulated aerosol amount (Section 3.1), size distributions (Section 3.2), and composition (Section 3.3), (b) perform an observation specific INP closure experiment (Section 4.1), and (c) evaluate simulated INP populations at the ocean surface (Section 4.2) and aloft (Section 4.3). In response to our findings, we discuss the influence of transported mineral dust on SO INP populations (Section 5.1) and new insights regarding representations of mineral dust INPs in remote regions (Section 5.2).

2. Methods

Here we describe the field observations used to evaluate simulated SO aerosol and INPs (Section 2.1) and a description of the Community Earth System Model version 2 (Section 2.2).

2.1. Southern Ocean Atmospheric Research Field Campaigns

Observations used in this study are from the Measurements of Aerosols, Radiation and Clouds over the Southern Ocean (MARCUS) campaign on the RV *Aurora Australis* between Hobart, Tasmania and the Australia Antarctic research stations south of Australia (McFarquhar et al., 2021). MARCUS voyages occurred from 21 October 2017–23 March 2018. This study also used airborne measurements made from the NSF/NCAR Gulfstream-V aircraft (GV, https://doi.org/10.5065/D6DR2SJP) during the Southern Ocean Cloud Radiation and Aerosol Transport Experimental Study (SOCRATES). SOCRATES included flights primarily targeting stratocumulus cloud decks south of Hobart, Australia, reaching as far south as 62°S during summertime (15 January to 26 February 2018). A map of the MARCUS and SOCRATES measurement tracks are provided in Figure S4 in Supporting Information S1.

Detailed observations of aerosol amount, aerosol composition, and ice nucleating particles from the MARCUS and SOCRATES campaigns are summarized in Table 1 and described in this section.

2.1.1. Observations of Aerosol Amount

During MARCUS, aerosol surface area (S_{tot}, µm² cm⁻³) was estimated using a Nephelometer (TSI Model 3563 Salwen et al., 2011), which measures scattering at wavelengths 450, 550, and 700 nm (Table 1). Following the approach from P. J. DeMott et al. (2016), the measured scattering coefficient (sP) and scattering efficiency (Q), estimated based on the calculated aerosol Angstrom exponent (Å), were used to estimate aerosol surface area following:

$$S_{tot} = 4\left(\frac{sP}{Q}\right), \quad \text{if Å} > 1; Q = 3; \quad \text{if Å} \leq 1; Q = 2. \tag{1}$$

This approach assumes all particles are spherical and that particles can be described from a single effective scattering size. During the MARCUS campaign, two particle impactors with 50% cutoff diameters of 1 and 10 µm,

were used alternately to measure surface area associated with particles with aerodynamic diameters smaller than 1 μm (PM1) and 10 μm (PM10), respectively. Particles were measured at ambient humidity and data included in this work only include measurements made at relative humidity lower than 35%. While ship exhaust is not expected to influence INP populations (McCluskey, Hill, Humphries, et al., 2018), exhaust can influence aerosol surface area. Nephelometer data contaminated by platform exhaust (∼85% of available data) were removed from the aerosol surface area data set, following Humphries et al. (2021).

During SOCRATES, size-resolved number concentrations of accumulation mode particles were measured using a wing-mounted Ultra-High Sensitivity Aerosol Spectrometer (WM-UHSAS, Droplet Measurement Technologies, Kupc et al., 2018; Laboratory, 2019b; Table 1). An additional UHSAS instrument (CVI-UHSAS) was located downstream of the counter flow virtual impactor (CVI) inlet (C. H. Twohy et al., 2021). The CVI inlet includes sampling modes for (a) in-cloud sampling of cloud particle residuals (i.e., particles remaining after evaporation of liquid or ice) or (b) ambient particles in cloud-free conditions (Noone et al., 1988). We determined validity of the WM-UHSAS data by comparing the two UHSAS's when the CVI-UHSAS was in ambient sampling mode. In this study, the first 5 bins of the WM-UHSAS sometimes included noise, thus size distributions were truncated to optical dry particle diameters between 0.07 and 1.0 μm. A 30-s running mean was also applied to the WM-UHSAS number size distributions to reduce noise. Number concentrations of particles within the truncated UHSAS size range (N_{UHSAS}) were determined by integrating the running mean UHSAS size distribution. Here, we only included data collected in conditions with <90% ambient relative humidity and note that the inlet de-icing heaters are expected to dry particles to <40% (Sanchez et al., 2021; Strapp et al., 1992), and we therefore considered particles detected by the UHSAS to be nominally dry and of clear or cloud-free air.

For coarse-mode sea salt aerosol, the NCAR Giant Nuclei Impactor (GNI) sampler (Jensen et al., 2020; Laboratory, 2019a) was used to collect particles with ambient aerodynamic diameters larger than 1.4 μm (Table 1). The GNI collects particles via impaction by exposing polycarbonate slides from the belly of the GV aircraft. Particle collections were primarily made within the marine boundary layer (Figure S5 in Supporting Information S1), with an aim of quantifying number size distributions of coarse mode sea salt particles. Collected particles were transported to NCAR (Boulder, Colorado) for analysis in the GNI optical microscope system, where collected slides were exposed to saturation ratios conducive to hygroscopic growth and subsequent droplet formation. Droplets formed from pure sea salt particles were identified by their uniform spherical shape and sea salt mass and dry particle radii were derived following methods described in detail in Jensen et al. (2020). These data were also used to determine integrated coarse mode sea salt number concentrations ($N_{SS,GNI}$).

2.1.2. Aerosol Composition Measurements

Single particle composition was monitored during the SOCRATES campaign by collecting particles for offline microscopic analysis, described by C. H. Twohy et al. (2021) (C. Twohy & Toohey, 2020) and summarized here (Table 1). Particles were collected onto grids via impaction downstream of the CVI inlet. Two size ranges were investigated in this study: (a) smaller particles (dry volume-equivalent diameter of about 0.1–0.5 μm) and (b) larger particles (0.5–5 μm). These physical diameters assume spherical particles with densities of 2 g cm^{-3} at 1,000 mb (C. H. Twohy et al., 2021). Particle size, morphology, and elemental composition were determined using analytical Scanning Transmission Electron Microscopy (STEM) and Energy Dispersive X-ray Spectroscopy (EDS) (See C. H. Twohy et al., 2021). Particle types identified using these analytical techniques included: (a) crustal, (b) sulfur, (c) organic, (d) metallic, (e) soot, (f) biomass burning, (g) Sea Spray—sodium dominated, (f) sea spray—high sulfur, and (g) Sea Spray—other. Crustal dust particles were distinguished from metallic particles dust particles based on the dominate presence of silicates and/or carbonates, whereas metals were dominated by aluminum, iron, chromium, titanium, manganese, cobalt, zinc, or copper. Organic particles were identified based on significant carbon signature with minor inorganic elements, while biomass burning particles were more dominated by potassium and sulfur as well as sometimes, detectable carbon. Chemical characterization was performed on 574 and 335 particles for the below and above cloud samples, respectively. The resulting particle type number fractions provide insight for influences of different particle types on the total particle population. This study uses the below-cloud and above-cloud aerosol composition results to assess simulated ambient aerosol composition.

2.1.3. Measurements of Ice Nucleating Particles

Number concentrations of immersion freezing INPs (n_{INPs}) were measured during the MARCUS and SOCRATES studies using the Colorado State University (CSU) ice spectrometer (IS, Barry, Hill, Jentzsch, et al., 2021; P. J. DeMott, 2018; P. J. DeMott et al., 2018). During MARCUS, total suspended ambient particles were collected onto

filters in open-faced filter holders that were approximately 18 m above the ocean surface (Table 1). Filters were exposed for 23–52 hr and the flow rate through the filters was monitored using a mass flow meter (TSI model 4043). While exhaust was present during the MARCUS sampling, we note that previous studies have reported no impact of exhaust on measured INPs (McCluskey, Hill, Humphries, et al., 2018). During SOCRATES, particles were collected below and above cloud using sterile aluminum filter holders (Table 1). Particles with diameters smaller than approximately 4 μm (Barry, Hill, Levin, et al., 2021; Eidhammer et al., 2010) were sampled below and above cloud (Figure S6 in Supporting Information S1) using an isokinetic inlet. Filters used in MARCUS and SOCRATES had pore sizes of 0.2 μm. Based on the flow rates achieved during SOCRATES (5.6–17.1 SL min^{-1}) and MARCUS (12.6–14.2 SL min^{-1}) and transmission calculations from Spurny and Lodge (1972), we expect filters to collect particles with diameters as small as 10 nm. Blank filters were collected during MARCUS and SOCRATES by preparing, handling, and storing filter units in the same manner as sample filters. MARCUS blank samples were also briefly exposed (with no vacuum) on the ship deck.

After collection during MARCUS and SOCRATES, particles were analyzed using the CSU IS. Particles were re-suspended into 6–8 mL of water, from which 50-μL aliquots were distributed into sterile 96-well PCR trays that were placed into the IS aluminum cooling block. Samples were cooled from room temperature to as cold as −28.5°C (−0.33°C min^{-1}), depending on the corresponding pure deionized water blank. Frozen fraction of wells were measured every 0.5–1°C and INP number concentrations (n_{INPs}) were determined following Vali (1971). For MARCUS and SOCRATES measured INPs were corrected for average background INPs detected on 3 and 6 blank filters, respectively. Measurements were considered below detection limit if corrected INP number concentrations or their 95% confidence interval was below zero.

Treatments were conducted on aerosol samples to determine the contributions of heat-labile and organic material to the total INP population. To heat-treat samples, a portion of the sample suspension was heated to 95°C for 20 min, cooled to room temperature and dispensed into the IS wells for analysis. To remove organic material from the sample solution, a hydrogen peroxide (H_2O_2) digestion at 95°C was performed following the methods described in McCluskey, Hill, Humphries, et al. (2018). Reductions in IN activity following heating or H_2O_2 digestion indicate the contributions of heat-labile and other organic material to the INP population, respectively. Results from these offline treatments are provided in Figure S7 in Supporting Information S1. We note that following heating, IN activity increased for one sample above the observed untreated range, particularly for IN temperatures greater than −20°C. This behavior has been previously observed in laboratory studies (McCluskey, Hill, Sultana, et al., 2018), but its origin is currently under investigation in other studies. We also note that we assume in our analysis no loss of surface area or number concentrations following heating or H_2O_2 treatments.

2.2. The Community Earth System Model, Version 2

The atmospheric component of the Community Earth System Model version 2 (CESM2), the Community Atmosphere Model version 6 (CAM6) was used to simulate aerosol properties during the MARCUS and SOCRATES periods. To replicate meteorological conditions, we utilized a specified dynamics configuration of CESM2 using a 24 hr relaxation time period to "nudge" simulated winds and temperature to the MERRA2 reanalysis data product. This model configuration interpolates the MERRA2 data to the standard 32 CAM vertical levels from the surface to 3 hPa (See Figure S8 in Supporting Information S1), uses a 30 min model time step with a 10 min microphysical sub-step, and has horizontal resolution of 0.9° latitude by 1.25° longitude. This configuration was found by Gettelman et al. (2020) to best reproduce the climate of CESM2 in a nudged configuration, using the same CAM levels and 24 hr nudging. CESM2 utilizes the Morrison-Gettelman two-moment microphysics scheme (Morrison & Gettelman, 2008) to treat cloud microphysics, which is coupled to a unified moist turbulence scheme, Cloud Layers Unified by Binormals (CLUBB), developed by Golaz et al. (2002) and Larson et al. (2002) and implemented in CAM by Bogenschutz et al. (2013). Simulations included over 10 months of spin up from 01 January 2017. An initial evaluation of simulated meteorology and clouds for SOCRATES using the model configuration used in this study was published in Gettelman et al. (2020).

To assess modeled aerosol and INP populations against observations, model output was archived along the flight and ship tracks at a 1 min resolution. Our analysis included co-located model data from the nearest model grid-box based on measurement latitude and pressure or altitude. Co-located data were binned based on latitude and altitude to determine biases in CESM2 aerosol spatial and vertical distributions. For filter and grid based measurements (IS, GNI, TEM grids), model data were collected during sampling periods. For example, the INP

measurements during MARCUS occurred over many hours and model data were sampled and averaged along the corresponding ship track.

2.2.1. Simulated Aerosol

Aerosol simulated in CESM2 follows the 2-moment modal aerosol model (MAM4, Liu et al., 2016), which includes six aerosol species: sea salt, mineral dust, black carbon, primary organic matter (POM), sulfate, and secondary organic aerosol (SOA). Aerosol species are emitted into four aerosol modes, including soluble Aitken mode (sea salt, sulfate, and SOA), soluble accumulation mode (mineral dust, black carbon, sea salt, POM, sulfate, and SOA), soluble coarse mode (mineral dust, sea salt, and sulfate), and insoluble primary carbon accumulation mode (black carbon and POM) (Liu et al., 2016). Each aerosol mode has a fixed modal width (σ_g) and a modal diameter (D_g) that evolves based on simulated physics. Mode-specific details are summarized in Table S1 in Supporting Information S1. In the release version of CESM2, MAM4 includes an updated coarse mode σ_g (1.2 vs. 1.8 used in CAM5) and larger size range (0.4–40 µm vs. 1–4 µm used in CAM5) that increases the lifetime of coarse mode aerosol including sea salt and dust aerosol (Li et al., 2022). To determine the influence of this change on simulated coarse mode aerosol over the Southern Ocean, we have performed a test experiment that reverted the coarse mode aerosol parameters to the CAM5 settings and results are described in Text S2 in Supporting Information S1. MAM4 includes cloud-borne aerosol and interstitial aerosol states; the model aerosol used in our analysis only included the simulated interstitial, or ambient/cloud-free, aerosol and were described with dry diameters. Aerosol species are assumed to be internally mixed, such that the number concentration of species x in mode m ($N_{x,m}$) is calculated using the modal mass fraction of species x multiplied by the total number concentration of the corresponding mode $N_{tot,m}$. Simulated aerosol surface area concentrations were determined from the simulated aerosol distributions assuming spherically shaped particles. Instrument simulators were created to "sample" matching size ranges of the modeled aerosol population. For example, bounded number concentrations were calculated for the size range of 0.07–1.0 µm to match the UHSAS size range.

The primary SO particle source, sea spray aerosol, is represented in CESM2 with sea salt aerosol with a hygroscopicity of 1.16. Ocean surface whitecap area is estimated in CESM2 based on windspeed following Monahan and Muircheartaigh (1980). Whitecap area and sea surface temperatures are used to determine sea salt flux according to Mårtensson et al. (2003) for sea salt particles with dry diameters between 0.020 and 2.8 µm. The Mårtensson et al. (2003) sea salt emission parameterization was developed based on measured sea salt aerosol size distributions generated via a sintered glass filter from laboratory synthetic seawater with temperatures of −2 to 25°C. The Monahan et al. (1986) parameterizations is used for particles with dry diameters between 2.8 and 10 µm. The organic component of sea spray aerosol is not currently represented in CESM2. Mineral dust aerosol emissions are simulated based on wind speed and soil aridity following Zender et al. (2003). While sea salt and mineral dust particles are interactive with modeled meteorology, all other aerosol species are emitted based on CMIP6 emission inventories (Gettelman, Mills, et al., 2019). Simulated aerosol loss processes include dry deposition, in-cloud scavenging, and below-cloud scavenging. In-cloud scavenging includes particles activated into cloud droplets and converted to rain via coalescence or accretion. In-cloud ice phase scavenging is not represented in CESM2.

2.3. Aerosol-Specific Deterministic INP Parameterizations

Measurements of n_{INPs} made during MARCUS and SOCRATES were used in this study to assess model skill for predicting INP abundance and type from three different parameterizations. Here, we focus on testing aerosol-specific deterministic INP parameterizations that ignore the stochastic, or time-dependent, nature of ice nucleation. This assumption is considered appropriate given that the microphysical time-step for climate models, including CESM2, is far larger than the timescale of ice nucleation (Vali et al., 2015). Previously, McCluskey et al. (2019) assessed CESM1 offline predictions of n_{INPs} against observed n_{INPs} from the CAPRICORN research voyage with a maximum latitude of −53°S. Here, we expand on the CAPRICORN study using more detailed aerosol measurements and respective instrument simulators and expand this assessment spatially, temporally, and vertically with data from the MARCUS and SOCRATES projects using CESM2. We also evaluate two different parameterizations for predicting INPs associated with mineral dust aerosol.

Multiple INP types have been identified in SSA: (a) an organic molecular marine INP type that coats sea salt particles and (b) a marine organic microbial INP type that is heat-labile and active at temperatures greater than

−20°C (McCluskey, Hill, Sultana, et al., 2018). In this study, we utilize the marine organic aerosol specific parameterization reported for pristine Atlantic marine air masses by McCluskey, Ovadnevaite, et al. (2018) (M18). M18 describes the INPs associated with the ice nucleation active organic molecules that coat sea salt particles. The M18 parameterization predicts n_{INPs} (in m^{-3}) based on temperature (T in Kelvin) and sea spray aerosol surface area concentration (S_{SSA} in m^2 m^{-3}, see Text S1 in Supporting Information S1):

$$n_{INPs,M18}(T) = \exp[-0.545(T - 273.15) + 1.0125] \times S_{SSA} \tag{2}$$

The M18 parameterization was used in this project to perform an observation closure study and to assess simulated n_{INPs}. For the observation closure study, marine organic aerosol measurements were not available and thus we assume that the sea spray aerosol surface area (i.e., sea salt + organic coatings) needed for M18 is approximately equal to total measured aerosol surface area from the nephelometer. Because CESM2 does not include a representation of marine organic aerosol, we assume in this work that organic coatings on sea salt particles minimally contribute to the total sea spray aerosol surface area. Therefore, simulated sea salt aerosol surface area and model temperature are used with M18 to predict INPs associated with sea spray aerosol in CESM2.

For mineral dust aerosol, we explore two commonly used deterministic mineral dust-specific INP parameterizations, including the Niemand et al. (2012) (N12) and the P. J. DeMott et al. (2015) (D15) parameterizations. The N12 parameterization predicts mineral dust INP number concentrations ($n_{INPs,N12}$ in m^{-3}) based on temperature (T in Kelvin) and available mineral dust aerosol surface area (S_{dst} in m^2 m^{-3}, see Text S1 in Supporting Information S1) and was derived using data from Aerosol Interactions and Dynamics of the Atmosphere expansion chamber cloud parcel experiments for temperatures ranging from −12 to −36°C:

$$n_{INPs,N12}(T) = \exp[-0.517(T - 273.15) + 8.934] \times S_{dst} \tag{3}$$

The D15 parameterization, developed using both laboratory and atmospheric data, predicts mineral dust INP number concentrations ($n_{INPs,D15}$ in L^{-1}) based on temperature (T in Kelvin) and number concentration of mineral dust particles larger than 500 nm ($n_{500nm,dst}$ in m^{-3}, see Text S1 in Supporting Information S1):

$$n_{INPs,D15}(T) = (cf)(n_{500nm,dst})^{\alpha(273.15-T)+\beta} \exp(\gamma(273.15 - T) + \delta), \tag{4}$$

where $\alpha = 0$, $\beta = 1.25$, $\gamma = 0.46$, $\delta = -11.6$ and $cf = 3$. Evaluation studies of the N12 and D15 parameterizations indicated that both parameterizations agree within a factor of 2 at temperatures lower than −25°C for mineral dust layer conditions, suggesting both parameterizations may be useful for predicting INPs associated with mineral dust aerosol (P. J. DeMott et al., 2015).

3. Simulating Southern Ocean Aerosol

3.1. Aerosol Abundance

Simulated surface level aerosol abundance during MARCUS was evaluated using the total aerosol surface area concentrations (S_{tot}) calculated from dry (RH < 35%) aerosol extinction as measured by a nephelometer (Figure 1a). Simulated aerosol surface area concentrations, derived from simulated aerosol size distributions, were determined for both PM1 and PM10 size ranges. Consistent with McCluskey et al. (2019), simulated S_{tot} followed observed S_{tot} (Figure 1a). While observed S_{tot} were within the interquartile range of simulated S_{tot} at all latitudes south of 48°S, observed S_{tot} were below the range of simulated S_{tot} north of 48°S. Simulated S_{tot} followed observed latitudinal variability, with observed and simulated S_{tot} exceeding 50μm^{2}cm^{-3} at latitudes north of 58°S and falling below 50μm^{2}cm^{-3} at latitudes south of 58°S. The high bias in simulated aerosol surface area concentrations relative to observations may be in part due to a high bias in coarse mode aerosol lifetime due to the large size range (0.4–40 μm) of the coarse mode aerosol used in CAM6. The high bias in aerosol surface area concentrations is reduced, though not fully resolved, when the MAM4 coarse mode aerosol parameters are reverted to the CAM5 values (Text S2, Figure S1 in Supporting Information S1). Simulated and observed temperatures and wind speeds were similar, with decreasing temperatures with increasing latitude and maximum wind speeds between 54° and 60°S. While simulated temperatures and wind speeds were consistent with observations for most latitudes, slightly lower simulated S_{tot} were associated with model surface level temperatures at or below 0°C (Figure 1c). The temperature-dependent sea salt emission scheme likely does not adequately represent particle fluxes from the ocean at temperatures lower than 0°C, as suggested by Mårtensson et al. (2003). Discrepancies
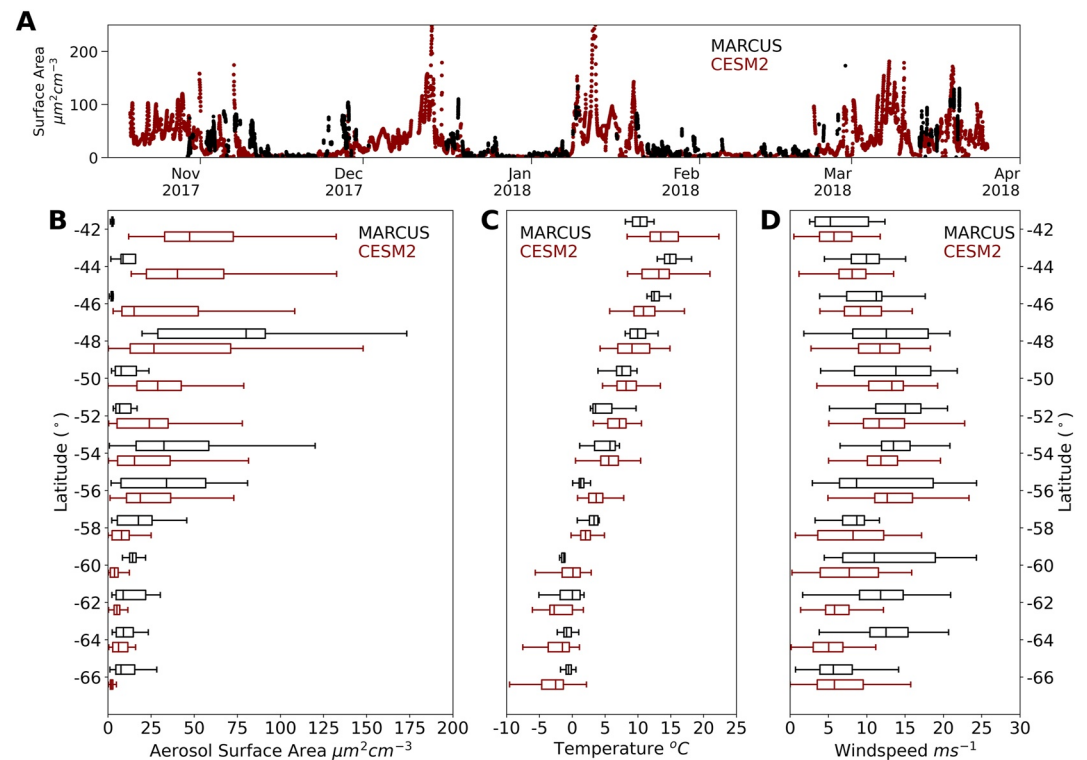
Figure 1. Observed and simulated aerosol surface area, surface temperature and surface wind speed during MARCUS. (a) Timeline of aerosol surface area during the MARCUS ship campaign. Observed aerosol surface area (black) was determined based on scattering detected by the nephelometer for all particles smaller than 10 μm (see Section 2.1.1). Simulated aerosol surface area (red) was derived for the simulated aerosol size distributions for particles smaller than 10 μm assuming dry spherical particles. Statistical boxplots describing the 25th, 50th, and 75th percentiles of the observed (black) and simulated (red) (b) aerosol surface area, (c) temperature, and (d) wind speed within 2° latitude bins. Observed temperatures and wind speeds were measured from the ship and simulated temperatures and winds are from the lowest model level.

near the sea ice edge may also have been due to simulated sea ice coverage where sea salt emissions were not predicted, or possibly the presence of local aerosol sources when the ship was at the Australian Antarctic stations. Overall, we report that S_{tot} simulated in CESM2 exceeded observed S_{tot} north of 48°S and followed the observed latitudinal decrease in S_{tot}.

During SOCRATES, accumulation mode aerosol number concentrations measured with the WM-UHSAS (N_{UHSAS}) were compared to number concentrations calculated from simulated aerosol size distributions truncated to match the UHSAS size range (Figure 2). Measured and simulated accumulation mode aerosol abundances were investigated within the model vertical levels (see Figure S8 in Supporting Information S1 for model vertical levels). Observed N_{UHSAS} maximized below 1 km, with median N_{UHSAS} ranging from 140 to 170 cm^{-3}. Simulated accumulation mode aerosol number during SOCRATES were underpredicted in CESM2 with median simulated N_{UHSAS} at altitudes below 1 km ranging from 59 to 84 cm^{-3}. Above 3 km, simulated N_{UHSAS} were also biased low compared to observed N_{UHSAS}, with observed and simulated median N_{UHSAS} ranging from 42 to 76 cm^{-3} and 9.0–17 cm^{-3}, respectively. Additionally, simulated N_{UHSAS} did not capture the variability of observed N_{UHSAS}. The overall vertical structure of accumulation mode aerosol abundance was replicated in the simulated aerosol, with a maximum in the marine boundary layer and lower concentrations aloft. However, discrepancies between simulated and observed N_{UHSAS} suggest a negative bias in simulated accumulation mode aerosol (0.07–1 μm) in the marine boundary layer and a negative bias in transported aerosol aloft.

Observed number concentrations of larger sea salt particles (N_{GNI}, dry diameters 1.4–32 μm) were determined by integrating measured number size distributions measured by the GNI during SOCRATES. Simulated N_{GNI} were also calculated from simulated sea salt aerosol number size distributions for the GNI size range (Figure 2). Large sea salt particles were highest at the lowest measurement altitudes, with median observed N_{GNI} ranging from 0.30 to 0.44 cm^{-3} below 0.5 km. Simulated large sea salt particles were biased high compared to those measured
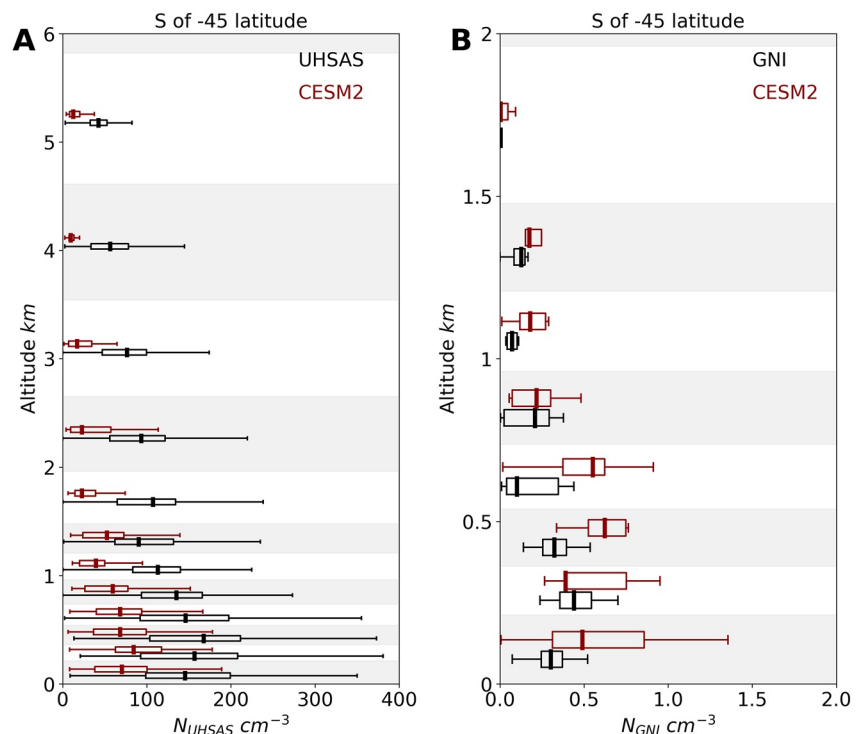
Figure 2. Vertical profile of number concentrations of (a) particles with dry diameters between 0.07 and 0.8 μm and (b) sea salt particles with diameters between 1.4 and 16 μm along the flight track for all latitudes south of −45°S. Observed concentrations (black) were measured by the (a) WM-UHSAS and the (b) GNI during SOCRATES. Co-located simulated bounded number concentrations were calculated for (a) all particles with dry diameters between 0.07 and 0.8 μm and (b) sea salt particles with dry diameters between 1.4 and 16 μm averaged over the GNI sampling period. Box plots illustrate the 5th, 25th, 50th, 75th, and 95th percentiles. Observed (black) and simulated (red) concentrations are binned within the mean model vertical layers.

by the GNI, with simulated N_{GNI} ranging from 0.39 to 0.62 cm^{-3} below 0.5 km. Simulated N_{GNI} was also more variable than observed N_{GNI} below 0.5 km, with a simulated N_{GNI} interquartile range of 0.31–0.86 cm^{-3} in the lowest model level. The high bias in simulated N_{GNI} relative to observations highlights an existing high bias in coarse mode aerosol lifetime due to the large size range (0.4–40 μm) of the coarse mode aerosol in MAM4. This bias is reduced when the coarse mode aerosol parameters are reverted to the CAM5 values (Text S2, Figure S2 in Supporting Information S1).

Biases between simulated and observed aerosol amount, including a positive bias in surface-level total aerosol surface area at latitudes north of 48°S, negative bias in accumulation aerosol number at all altitudes assessed, and high bias in coarse mode aerosol, are investigated further with aerosol size distributions and aerosol composition in Section 3.2.

3.2. Aerosol Size Distributions

To further understand biases in simulated aerosol amount described in Section 3.1, we evaluated simulated aerosol size distributions against observations. Aerosol size distributions were measured with the WM-UHSAS (Figures 3a–3c) and GNI (Figures 3d–3f) during SOCRATES. Simulated aerosol size distributions were reconstructed from the simulated co-located modal distribution parameters. In MAM4 used in CAM6, simulated modal dry diameter and number concentrations evolve with model physics and modal widths are constant. Observed and simulated average size distributions were determined for cloud-free measurements made within the marine boundary layer (MBL, 100–400 m), above cloud (1,100–1,800 m), and the upper troposphere (4,500–6,900 m).

In the MBL and above cloud (Figures 3a and 3b), simulated number concentrations for particles with dry diameters between 0.2 and 0.5 μm align with observed number concentrations. However, for particles with dry
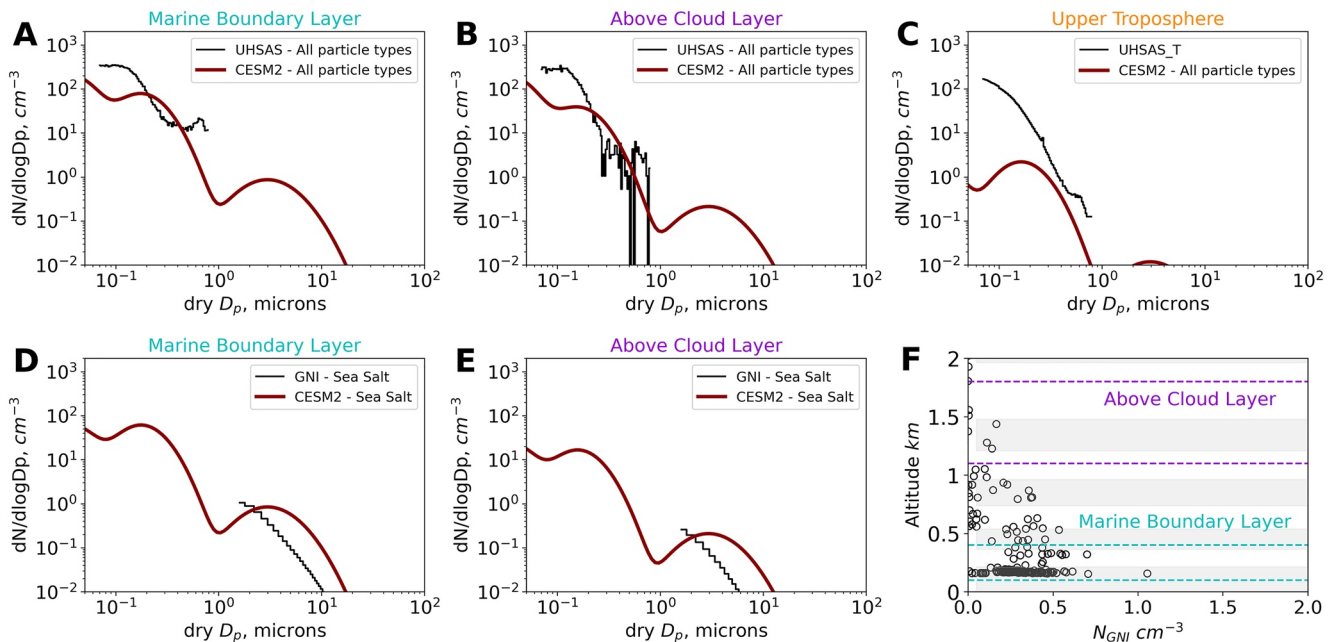
Figure 3. Average UHSAS (black) and simulated (red) aerosol number size distributions for the (a) marine boundary layer (100–400 m), (b) above clouds (1,100–1,800 m), and (c) upper troposphere (4,500–6,900 m) during SOCRATES. Simulated distributions in a–c include all simulated particle types. UHSAS and CAM6 distributions include all data along the GV flight path within the geopotential height ranges and with <90% relative humidity. Simulated distributions in d and e include only simulated sea salt particles, along with GNI observations, for the (d) marine boundary layer (100–400 m) and (e) above cloud (1,100–1,800 m). The vertical distribution of GNI aerosol number concentrations are provided in f with the altitude bounds for "Above cloud layer" and "Marine Boundary Layer" indicated.

diameters between 0.07 and 0.2 μm, simulated concentrations are a factor of 10 lower than observed. Observations indicate an accumulation mode modal diameter of approximately 0.15 μm, whereas the CAM6 aerosol size distribution minimizes at approximately 0.1 μm (between the Aitken and accumulation modes). In the upper troposphere (Figure 3c), simulated accumulation mode aerosol biases are similar to the MBL and above cloud measurements, with a negative bias of a factor of 10–100 in simulated aerosol smaller than 0.2 μm compared to the WM-UHSAS measurements. The negative bias in small particles is consistent with the negative bias in N_{UHSAS} discussed in Section 3.1.

Large sea salt aerosol measurements provided by the GNI were also used to compare simulated coarse mode sea salt aerosol size distributions within the MBL and above the cloud layer (Figures 3d and 3e). Both in the MBL and the above cloud layer average distributions highlight a high bias in simulated sea salt particles larger than 2 μm. The high bias in simulated coarse mode sea salt aerosol is consistent with the high bias in coarse mode aerosol lifetime due to the large coarse mode size range (0.4–40 μm) and this bias is reduced when the coarse mode aerosol parameters are reverted to the CAM5 values (Text S2, Figure S3 in Supporting Information S1).

3.3. Aerosol Composition

Finally, we used airborne measurements of aerosol composition, previously reported by C. H. Twohy et al. (2021), to assess simulated aerosol composition and understand biases. C. H. Twohy et al. (2021) reported single-particle chemical and morphological analyses of two particle size ranges: smaller particles ($0.1 < D_p < 0.5$ μm) and larger particles ($0.5 < D_p < 5$ μm). Particles were collected below cloud in the MBL, in non-precipitating clouds (as cloud particle residuals), and above cloud during SOCRATES. These data include number fractions of particle types within the reported size ranges and are used here to assess cloud-free below cloud and above cloud aerosol types simulated by CESM2 from the same location and time (Figure 4).

In all but one below cloud sample, observed smaller particles (0.1–0.5 μm) were dominated (60%–99%) by sulfur particles (Figure 4a). Sulfate particles may be from in-cloud heterogeneous chemical processing (Feingold & Kreidenweis, 2000). Previous studies have also indicated that these sulfur particles may result from new particle formation and growth from marine biogenic gaseous precursors (C. H. Twohy et al., 2021; McCoy et al., 2021). Observed smaller particles also included contributions (10%–55%) from sea spray particles below cloud. Below
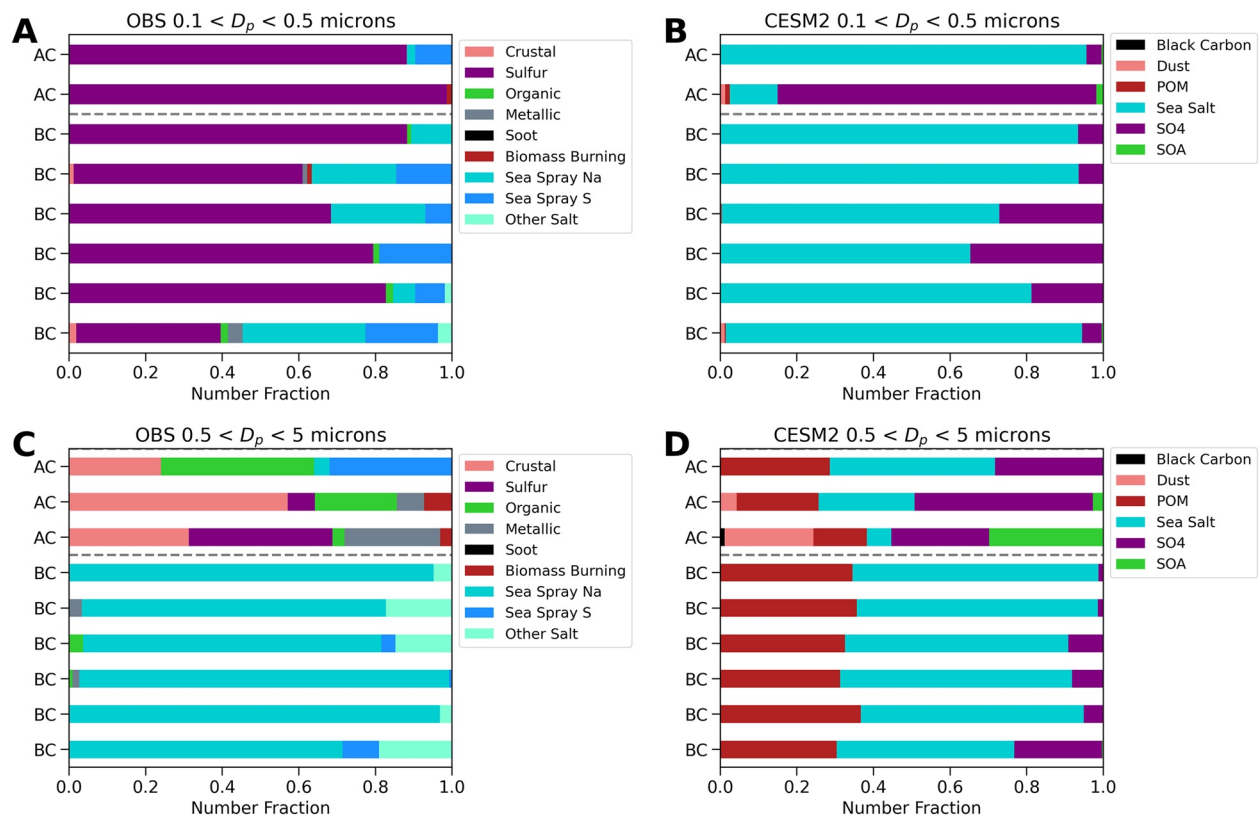
Figure 4. Observed number fraction of aerosol particle types for (a) particles with diameters 0.1–0.5 μm and (c) particles with diameters 0.5–5 μm, analyzed and reported by Twohy et al. (2021). Samples were collected below-cloud (BC) and above-cloud (AC) during the SOCRATES campaign and identified based on their chemical makeup and morphology. Co-located CESM2 aerosol data were selected to match the time periods and locations of observations for (b) particles with diameters 0.1–0.5 μm and (d) particles with diameters 0.5–5 μm. Colors indicate the particle type either based on the chemical and morphology analysis or predicted from CESM2.

cloud, simulated smaller particles from CESM2 (Figure 4b) were dominated by sea salt particles (65%–95%) and included contributions from sulfate aerosol. Similar to findings reported in McCoy et al. (2021), CESM2 consistently underestimated the sulfur aerosol contribution to the small particle population. In all above and below cloud samples, minimal contributions from land-derived aerosol (mineral dust, metallic, soot/black carbon, POM) were detected in observed and simulated small aerosol populations.

Observed larger particles (0.5–5 μm) below cloud in the MBL were dominated by sea salt particle types (96%–100%), whereas larger particles observed above cloud included crustal (24%–57%), biomass burning (3%–7%), and metallic (0%–25%) particles (Figure 4c). These land-derived particle types were likely from long-range transport. Organic particles, with possible sources from land or ocean, were also detected above cloud (3%–40%) and in one below cloud sample (4%). Simulated larger particle populations below cloud were dominated by sea salt particles (46%–64%) and were also influenced by land-derived aerosol. Specifically, 30%–37% of the simulated larger particle populations sampled below cloud were POM, emitted from biomass burning and fossil fuel combustion. Above cloud, mineral dust was predicted by CESM2 (Figure 4d) for 2 of 3 sampling periods (4% and 23%) compared to all 3 observed samples containing mineral dust or crustal particles.

To summarize, compared to the MARCUS and SOCRATES observations, we identify several biases in the release version of CESM2 regarding SO interstitial aerosol: (a) too few accumulation mode sulfur particles throughout the atmospheric column, (b) too high surface-level aerosol surface area concentrations at latitudes north of 48°S, (c) too many sea salt particles larger than 1.4 μm in the MBL, (d) too persistent particulate organic matter below cloud, and (e) large uncertainties in above cloud aerosol abundance and type (especially mineral dust). A negative bias in simulated sulfur particles smaller than 0.2 μm in CESM2 is consistent with McCoy et al. (2021), who demonstrated this bias leads to an under prediction of cloud droplet number concentrations and subsequent cloud microphysics and radiative properties. However, sulfur particles are not expected to influence the immersion freezing INP budget.

Additionally, POM particles are not currently active as INPs in CESM2 and are not considered an important INP source in this study. While model biases in sulfate and POM are both important to address for representing CCN populations, investigating these is beyond the scope of this study. High biases in coarse mode sea salt surface area concentrations were moderately reduced when the coarse mode aerosol size range was reverted to the CAM5 coarse mode size range (1–4 μm, Text S2 in Supporting Information S1). The biases in simulated mineral dust and sea salt particles are important to consider as they drive INP parameterizations and so will impact model-predicted INP populations.

4. Simulating Southern Ocean Ice Nucleating Particles

4.1. INP Closure From Observed Aerosol Surface Area

We first aim to reproduce observed n_{INPs} from MARCUS under the assumption that the INP population was entirely comprised of marine organic aerosol described by the M18 parameterization. In our observation closure study, we use aerosol surface area estimated from the nephelometer and assume that all aerosol surface area is sea spray aerosol (i.e., $S_{SSA} \approx S_{neph}$). We use the two inlet impactors on the nephelometer (PM10 and PM1) to determine the influence of particles with diameters <1 μm versus <10 μm. One limitation of the M18 parameterization is that it was derived from n_{INPs} measured from pristine Atlantic marine air masses that lacked the heat-labile marine INP type. To determine the role of heat labile ice nucleation material on the measured INP populations, we also repeated the observation closure study using the heat treated INP results (See Section 2.1.3). We note that uncertainties in aerosol surface area estimated from the nephelometer were not quantified due to a lack of an independent surface area measurement, but will contribute to variability and uncertainty in this observation closure study.

n_{INPs} predicted using M18 and observed aerosol surface area of PM10 were within a factor of 10 of observed n_{INPs} with a high bias of 20% ($B_n = 0.20$) (Figure 5b). Using PM1 aerosol surface area instead (Figure 5a), bias in predicted n_{INPs} shifted to a negative bias of 21% ($B_n = -0.21$), suggesting supermicron aerosol contributes to but does not dominate INPs predicted using M18. Using n_{INPs} measured from heated samples collected during the MARCUS campaign, we assessed the predictive skill of M18 when excluding the heat-labile INPs (Figures 5c and 5d). While many of the n_{INPs} measured at temperatures greater than −15°C are significantly lowered after heating, the modified normalized mean bias is unchanged when we only consider the heat-stable material and use the measured PM10 S_{neph} (Figure 5d). When considering only PM1 S_{neph} compared to PM10 S_{neph}, the B_n improves from 0.20 to −0.09 (Figure 5c).

Overall, the agreement, within a factor of 10, between predicted n_{INPs} and observed n_{INPs} in these observation closure studies suggest that the dominant INP source in the marine boundary layer is likely from marine organic aerosol described by M18. Negative B_n suggests that INP populations were not entirely described by M18, and heat-labile marine INPs or other INP types also likely contributed to the measured SO INP population.

4.2. Simulated Surface-Level INP Populations

In this study, CESM2-predicted INP populations were assessed against observed n_{INPs} by applying the M18, N12, and D15 parameterizations to simulated S_{ss}, S_{dst}, and $n_{500nm,dst}$, respectively. Further, we utilize treated samples provided from MARCUS to investigate contributions of heat-labile and organic materials to the INP populations, as summarized in Table 2 and provided in Figure S9 in Supporting Information S1. Previous model-observation comparisons used the M18 and D15 parameterizations applied to simulated aerosol from a modified version of CAM5 that included a representation of marine organic aerosol (McCluskey et al., 2019). Simulated marine organic aerosol particles are not included in this version of CESM2. Here, S_{SSA} is approximated using the total simulated sea salt surface area (S_{ss}).

Model-predicted n_{INPs} using M18 and simulated S_{ss} for MARCUS are biased low ($B_n = -0.65$) compared to untreated observations (Figure 6a). This bias is improved ($B_n = -0.40$) when model-predicted INPs are compared to heat-stable INPs (heated samples, Figure 6b), suggesting the heat-stable INP populations are dominated by marine INPs described by M18, consistent with the observation closure analysis (Section 4.1). However, agreement between observed and model-predicted n_{INPs} is significantly variable, with only 30% of the model-predicted n_{INPs} within a factor of 2 of observed n_{INPs}. This variability is largely controlled by disagreements between simulated and nephelometer-derived S_{tot}, and more specifically a consistent negative bias in simulated S_{tot} compared to observed S_{tot} (Figure S10 in Supporting Information S1).

The surface-level observations and the observational closure study results (Section 4.1) indicate that marine aerosol dominated the SO marine boundary layer INP population. However, previous modeling studies have suggested long-range transported mineral dust aerosol may influence SO INP populations aloft. Additionally, C.
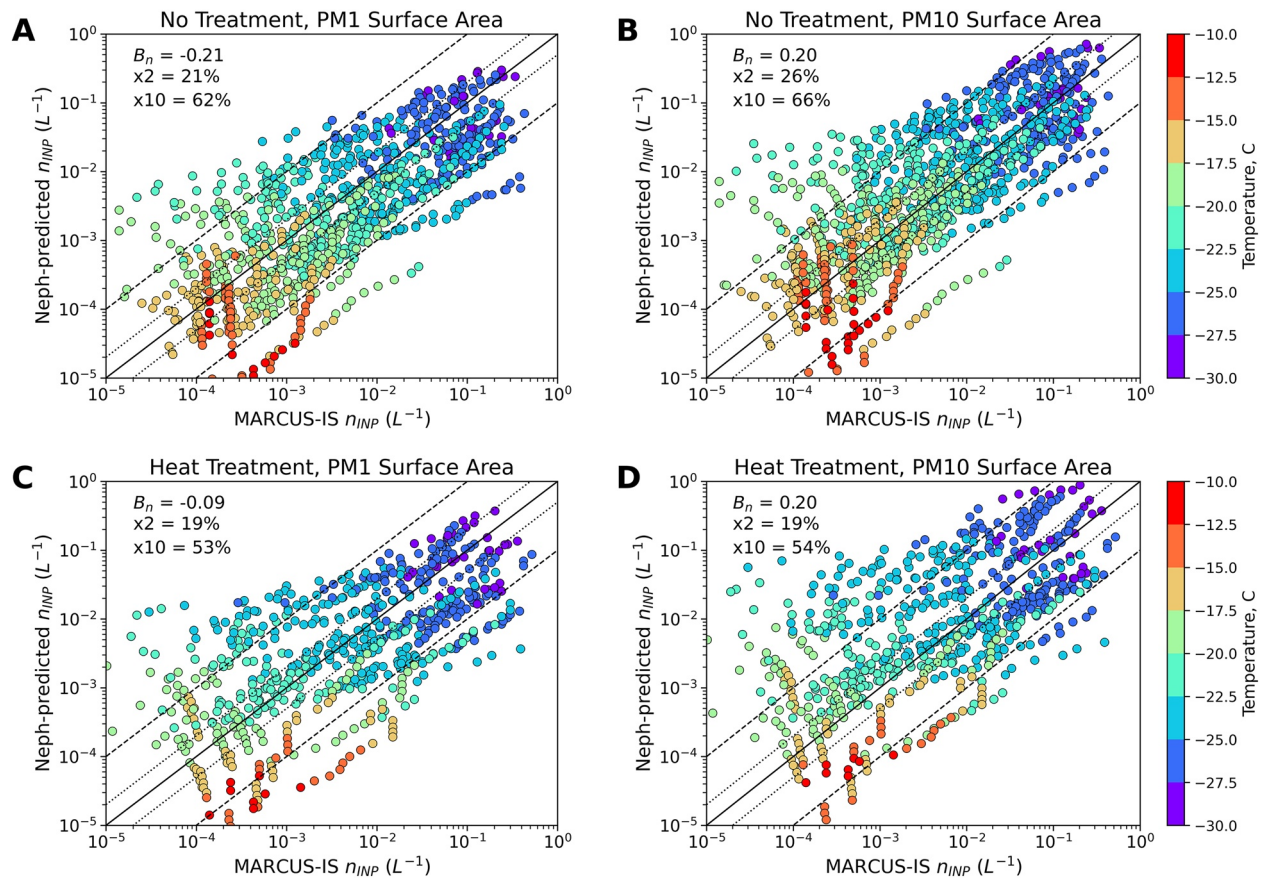
Figure 5. Ice nucleating particle number concentrations (n_{INPs}) predicted using M18 and aerosol surface area S_{neph} estimated from the nephelometer for all particles smaller than 1 μm (PM1, a and c) and all particles smaller than 10 μm (PM10, b and d) from the MARCUS campaign. All observed n_{INPs} are for untreated samples in a and b. All observed n_{INPs} are for heated samples in c and d. Colors indicate the ice nucleation temperature. The one-to-one line is indicated with the solid black line, with a factor of 2 (10) also shown in the dotted (dashed) lines. Modified normalized mean bias (B_n) and the percentage of points within a factor of 2 (×2) or 10 (×10) are also shown for each comparison.

Table 2
Bias Metrics for n_{INPs} Comparisons as Described in Sections 4.1, 4.2, and 4.3

| Study	Observed n_{INPs}	INP assumption	Predicted n_{INPs}	B_n	×2	×10
MARCUS *Observation-Closure*	No treatment	Marine INPs	M18(PM1)	−0.21	21%	62%
	No treatment	Marine INPs	M18(PM10)	0.20	26%	66%
	Heated	Marine INPs	M18(PM1)	−0.09	19%	53%
	Heated	Marine INPs	M18(PM10)	0.20	19%	54%
MARCUS *Model-Predictions*	No treatment	All INPs	M18	−0.65	32%	79%
	No treatment	All INPs	M18 + N12	0.73	30%	67%
	No treatment	All INPs	M18 + D15	−0.50	30%	80%
	Heated	Heat-stable INPs	M18	−0.40	30%	74%
	Heated	Heat-stable INPs	M18 + N12	0.94	16%	55%
	Heated	Heat-stable INPs	M18 + D15	−0.24	31%	73%
	H_2O_2	Refractory INPs	M18	0.46	28%	69%
	H_2O_2	Refractory INPs	N12	1.31	14%	35%
	H_2O_2	Refractory INPs	D15	−0.91	7%	40%
SOCRATES *Model-Predictions*	No treatment	All INPs	M18 + D15	−0.93	14%	46%
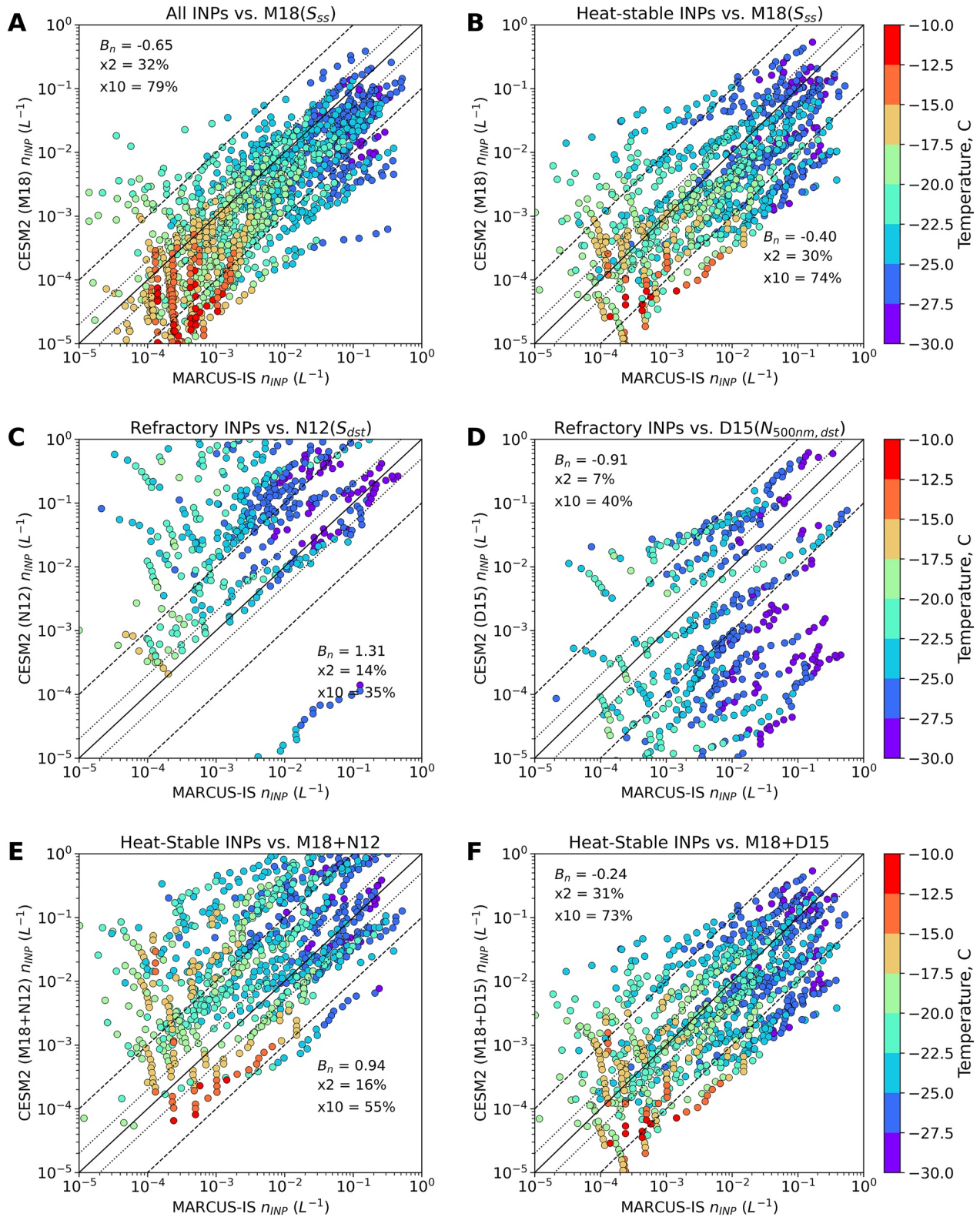
Figure 6.

H. Twohy et al. (2021) reported that 26% of the 87 individual INPs (active between −27 and −32°C) analyzed from samples collected from ship and aircraft were crustal/metal particles (Figure 4 in C. H. Twohy et al., 2021). The remaining n_{INPs} after H_2O_2 treatment applied to the collected INP populations suggests refractory INPs do contribute to the measured INP population, particularly at temperatures lower than −20°C (Figure S7 in Supporting Information S1). As such, we assess the use of the N12 and D15 parameterizations against the observed refractory INPs (Figures 6c and 6d). Model-predicted INPs using N12 with simulated S_{dst} are biased high ($B_n = 1.31$) compared to H_2O_2 treated n_{INPs}. By contrast, n_{INPs} estimated using D15 applied to simulated $n_{500nm,dst}$ are biased low ($B_n = -0.91$) compared to H_2O_2 treated n_{INPs}. Over 4 orders of magnitude variability in n_{INPs} is estimated, with only 14% and 7% of model-predicted n_{INPs} within a factor of 10 of observed n_{INPs} using N12 and D15, respectively, highlighting significant deviations of model-predicted mineral dust INPs from observed refractory INPs.

Considering an INP population comprised of marine and mineral dust INPs, model-predicted marine (M18) and mineral dust (N12 or D15) INPs are compared to heated n_{INPs} (Figures 6e and 6f). Consistent with the high bias of the N12 predicted refractory INPs, the M18 + N12 approach is biased high with a $B_n = 0.94$ compared to heat-stable n_{INPs} observations. Using the D15 approach for the mineral dust component is biased high ($B_n = 0.24$) compared to heat-stable n_{INPs} observations. While both N12 and D15 have been illustrated to provide similar results when used to estimate mineral dust INPs in laboratory and field measurements of mineral dust plumes, these two INP estimates are drastically different over the remote Southern Ocean. This is discussed further in Section 5.2.

4.3. Vertical Complexities in Southern Ocean INP Populations

Measurements of n_{INPs} below and above cloud during SOCRATES provide some of the first observational insights into INP populations above the ocean surface in this region. Aerosol filter samples were collected during multiple exposures between 45 and 62°S (Figure S6). Based on results from Section 4.2 and McCluskey et al. (2019), the M18 + D15 approach is used to estimate model-predicted INPs (Figure 7a). Model-predicted n_{INPs} are lower than n_{INPs} observed during SOCRATES with a B_n of −0.93 and significant variability in predictive ability, with 54% of model-predicted n_{INPs} more than a factor of 10 different from observed n_{INPs}.

The influence of simulated mineral dust aerosol on model-predicted INPs is determined by using the ratio of simulated marine INPs and simulated mineral dust INPs $\left(\log\left(\frac{n_{INPs,M18}}{n_{INPs,D15}}\right)\right)$, where ratios greater (lower) than 0 are marine-dominated (mineral dust-dominated) INP populations. For marine-dominated INP populations, model-predicted n_{INPs} are consistently biased low ($B_n = -1.25$, Figure 7b), consistent with negative biases in accumulation mode aerosol (Figure 2). While simulated mineral dust-dominated INP populations are associated with a bias of only 0.26, only 28% of model-predicted n_{INPs} are within a factor of 10 of observed n_{INPs} (Figure 7c).

Approximately 20% (7 of 32) of samples from SOCRATES correspond to simulated INP populations dominated by mineral dust INPs, ranging from the MBL up to 6 km (Figure S6 in Supporting Information S1). All simulated samples above 3 km ($N = 4$) are mineral dust-dominated. Without additional aerosol composition and INP analysis, it is unclear if the simulated INP types agree with the observed INP types. However, the up to four orders of magnitude variability associated with the predicted mineral dust-dominated INP populations (Figure 7c) suggests that simulated mineral dust aerosol is a significant uncertainty in predicting Southern Ocean n_{INPs}.

5. Discussion

5.1. Mineral Dust Influence on Southern Ocean INP Populations

Offline treatments of INPs sampled during MARCUS are one of the only measures of refractory, or mineral dust, INPs over the Southern Ocean region to date. The air mass origins associated with the four highest refractory n_{INPs} filter periods were determined using back trajectories estimated using the HYSPLIT model (McFarquhar et al., 2021, released at 1 km, Figure 8). One of the samples with elevated refractory n_{INPs} was collected near Tasmania with air masses originating from Australia. Three of the samples with elevated refractory n_{INPs} were

Figure 6. Comparisons between model-predicted (CESM2) and observed (MARCUS) INP number concentrations (n_{INPs}). Observed n_{INPs} are for untreated samples (i.e., the full INP population) in panel (a). Observed INP number concentrations are for heat-stable INPs (i.e., heat treated) in panels (b, e, and f). Observed n_{INPs} are for refractory INPs (H_2O_2 treated) in panels (c and d). Marker colors indicate the ice nucleation measurement temperature. Parameterizations used to predict n_{INPs} are included in each panel. Model predicted n_{INPs} were determined based on the co-located S_{ss}, S_{dst}, or $N_{500nm,dst}$ as input to the M18, N12, and D15 parameterizations, respectively, as described in Section 2.3. The one-to-one line is indicated with the solid black line, with a factor of 2 (10) also shown in the dotted (dashed) lines. Modified normalized mean bias (B_n) and the percentage of points within a factor of 2 (×2) or 10 (×10) are also provided for each comparison.
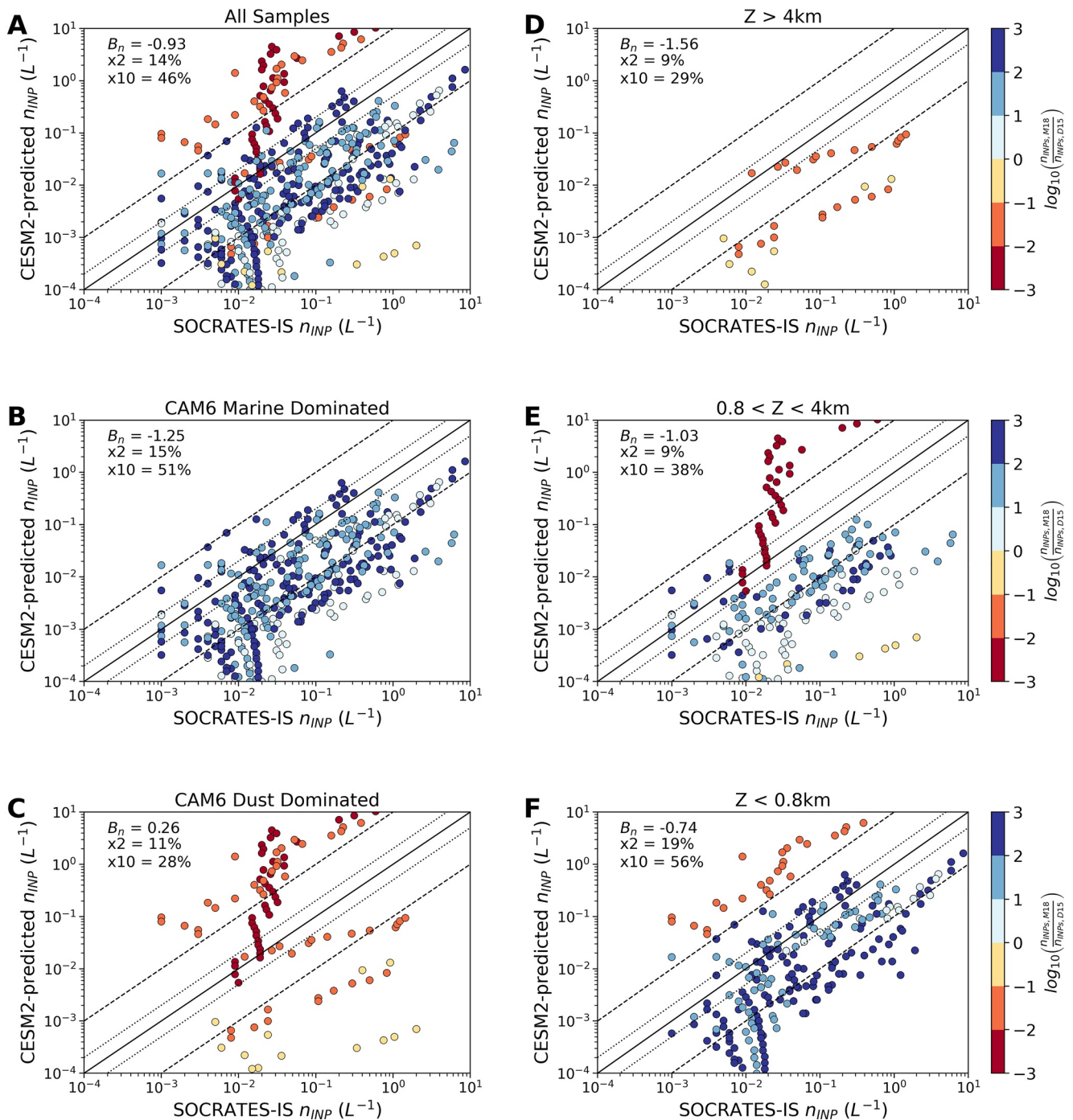
Figure 7. Comparisons of INP number concentrations (n_{INPs}) predicted using CESM2 simulated aerosol as input to the M18 and D15 parameterizations (See Section 2.3) compared to measured n_{INPs} from SOCRATES. The one-to-one line is indicated with the solid black line, with a factor of 2 (10) also shown in the dotted (dashed) lines. Marker colors in all panels (a–f) correspond to the simulated ratio of marine INPs to mineral dust INPs as predicted by M18 and D15, respectively (a) includes all data, (b) includes samples with simulated INP populations dominated by the marine (M18) INP source and (c) includes samples with simulated INP populations dominated by the mineral dust (D15) INP source. In d–f, samples are segregated into average sampling altitude (d) greater than 4 km, (e) between 0.8 and 4 km, and (f) below 0.8 km. Modified normalized mean bias (B_n) and the percentage of points withing a factor of 2 (x2) or 10 (x10) are also provided for each comparison.

samples collected at higher latitudes, including one collected near an Australian Antarctic Station. Back trajectory analysis suggests that these samples were often associated with air masses originating from the edge of Antarctica or high southern latitudes. While mineral dust originating from Antarctica may be possible, the presence of refractory INPs, particularly over the open ocean, is surprising. We note that the version of CESM2
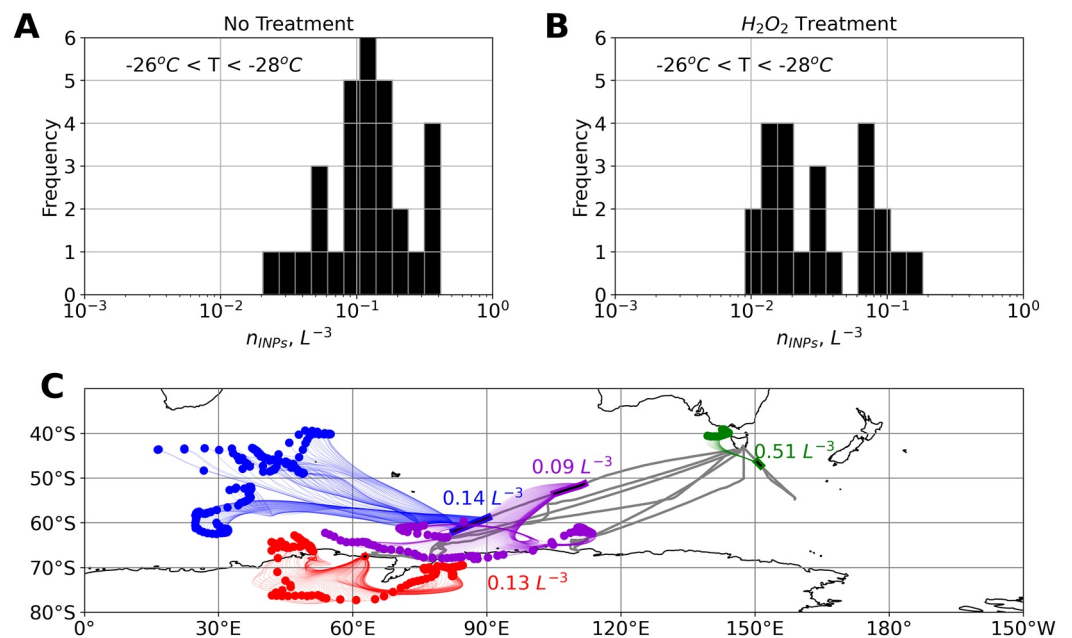
Figure 8. Distribution of average n_{INPs} measured between -26 and $-28°C$ during MARCUS for (a) untreated samples and (b) H_2O_2 treated samples (i.e., refractory INPs). Sample locations along the MARCUS ship track for samples associated with the four highest refractory n_{INPs} are shown in (c) in unique colors along the MARCUS ship track (gray link). The 72 hr back trajectories (colored lines) and endpoints (points) estimated using the HYSPLIT model (release point 1,000 m from McFarquhar et al. (2021)) are also shown. The refractory n_{INPs} measured between -26 and $-28°C$ are provided for these four samples in text in panel (c) in colors corresponding to the trajectory colors. The MARCUS ship track is indicated by the gray line.

used in this study does not include mineral dust emissions from Antarctica. Detailed bacterial profiling from a ship-campaign during the same period as SOCRATES reported by Uetake et al. (2020) indicated that the SO marine boundary layer is pristine, with little to no influence from continental regions. Re-suspension of mineral dust particles from the ocean surface via bubble bursting has been proposed based on laboratory studies of synthetic seawater doped with mineral dust (Cornwell et al., 2020). While the majority of INPs measured in the marine boundary layer are of marine origin, our results suggest that mineral dust aerosol sources and transport are likely key aspects of the INP populations over the southern high latitudes currently, and perhaps in the past and future.

5.2. Representing Mineral Dust INPs in Remote Regions

A challenge in representing INPs in a global scale model is the dependence on many aerosol processes to achieve reasonable aerosol abundances and composition. The SO is one of the most pristine regions in the world with regard to INPs and has a high occurrence of liquid-dominated mixed phase clouds. As such, cloud radiative properties may be highly sensitive to small perturbations in INP populations (Raatikainen et al., 2022; Vergara-Temprado et al., 2018; Vignon et al., 2021). Mineral dust is associated with three orders of magnitude greater ice nucleation site densities compared to marine aerosol (P. J. DeMott et al., 2016), such that very small amounts of mineral dust aerosol can significantly influence simulated INP populations. Here, we discuss the nuances associated with representing mineral dust INPs in remote regions.

Initial comparisons between model-predicted and observed n_{INPs} (Section 4.3) revealed significant differences between two commonly used mineral dust INP parameterizations (D15 and N12). An important difference between D15 and N12 is that D15 considers only mineral dust particles with diameters larger than 500 nm ($n_{500nm,dst}$), whereas N12 is related to the total mineral dust aerosol surface area (S_{dst}). Aerosol quantities that correspond to the observed upper limit of n_{INPs} at $-20°C$ over the SO ($n_{INPs,-20} = 0.1$ L^{-1}, Figure S7 in Supporting Information S1) are $n_{500nm,dst}$ of 0.45 cm^{-3} and S_{dst} of 0.43 μm^{2}cm^{-3}. Simulated zonal monthly averaged values of $n_{500nm,dst}$ and S_{dst} are presented in Figure 9 and demonstrate different global influences of mineral dust INPs. For $n_{500nm,dst}$, the highest concentrations are near latitudes with known mineral dust sources and do not exceed
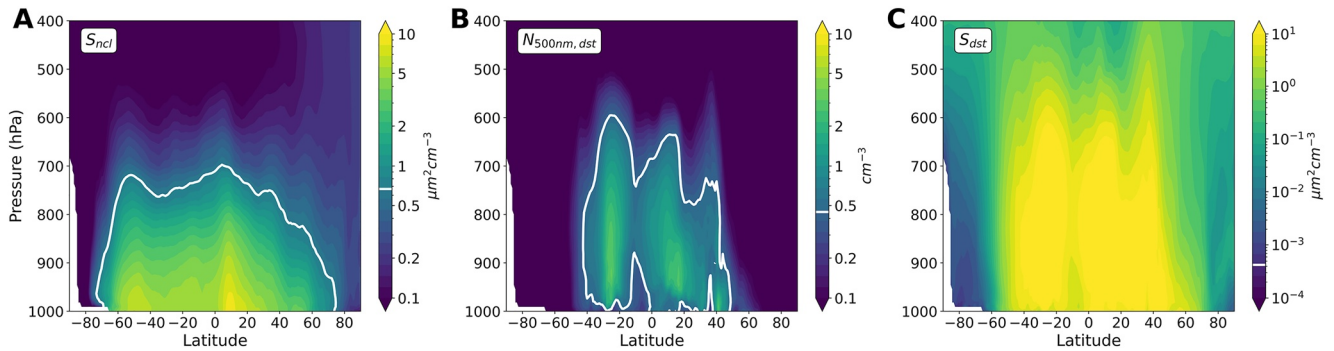
Figure 9. Zonal monthly mean of simulated aerosol quantities used as input to the (a) M18 (S_{ss}) (b) D15 ($n_{500nm,dst}$), and (c) N12 (S_{dst}) INP paramterizations for February 2018. Aerosol values corresponding to predicted n_{INP} equal to or greater than n_{INP} at $-20°C$ ($n_{INPs,-20} = 0.1$ L^{-1}) are outlined by the white contour line. The lower S_{ss} threshold corresponding to $n_{INP,-20} = 0.1$ for M18 is 670 µm^{2}cm^{-3}. The lower $n_{500nm,dst}$ threshold corresponding to $n_{INP,-20} = 0.1$ for D15 is 0.45 cm^{-3}. The lower S_{dst} threshold corresponding to $n_{INP,-20} = 0.1$ for N12 is 0.43 µm^{2}cm^{-3}. Note that all simulated S_{ss} were lower than 670 µm^{2}cm^{-3} (i.e., there is no visible white contour in panel (a)).

0.45 cm^{-3} below 5 km south of 50°S. By contrast, S_{dst} exceeds 0.43 µm^{2}cm^{-3} globally between 60°S and 70°N, indicating that applying N12 to simulated S_{dst} will result in mineral dust aerosol dominating INP populations globally. While mineral dust INPs predicted using D15 and N12 are consistent when used in conditions with high mineral dust concentrations (P. J. DeMott et al., 2015), these results indicate that using N12 globally will overestimate mineral dust INPs in regions removed from mineral dust sources. We note that both D15 and N12 were developed under aerosol loading exceeding these thresholds, with $n_{500nm,dst}$ exceeding 1 cm^{-3} (P. J. DeMott et al., 2015) and S_{dst} exceeding 50 µm^{2}cm^{-3} (Niemand et al., 2012). As such, this analysis reveals a limitation of agreement between D15 and N12 in regions far removed from mineral dust sources and thus should be use cautiously in modeling studies (Figure S11 in Supporting Information S1). This limitation of agreement between D15 and N12 also has consequences on observational studies far-removed from mineral dust sources that aim to develop parameterizations or use aerosol-specific parameterizations for INP source apportionment.

Previous modeling efforts focused on the direct aerosol effect of mineral dust which required an assessment of mineral dust optical properties near mineral dust sources that can often be measured from satellite (e.g., Wu et al., 2019). However, the ability to represent the sensitive interplay between mineral dust INPs and marine INPs over the SO depends on the ability to accurately simulate mineral dust and marine aerosol number and size. Realistic representations of aerosol-cloud interactions, with aerosol amount and composition influencing cloud activation, ice nucleation, and subsequent cloud microphysics and radiation, is a promising advancement for Earth system modeling. However, future observational studies need to include measurements that target aerosol composition and aerosol transport processes, including quantitative mineral dust aerosol measurements in regions far removed from mineral dust sources.

6. Summary

In this study, three deterministic INP parameterizations that describe marine INPs (M18) and mineral dust INPs (D15 and N12) were assessed for use in the Community Earth System Model version 2. This study was motivated by the need to represent marine INP sources over the Southern Ocean and a desire to replace the current CNT IN parameterization with one that can be easily evaluated against INP measurements.

In order to accurately predict INPs, models must first accurately simulate the abundance and type of INP aerosol sources. As such, we evaluated total surface-level aerosol surface area, accumulation model aerosol number concentrations and size distributions, coarse model sea salt aerosol, and aerosol composition in two size ranges. Based on these analyses, we find that CESM2 includes many biases in representing SO aerosol: (a) too few accumulation mode sulfur particles, (b) too persistent POM aerosol below cloud in the MBL, (c) too high surface-level aerosol surface area north of 48°S and (d) too many sea salt particles larger than 1.4 µm. Biases in sulfur and POM do not currently influence INP predictions, because they are not considered to be IN active in CESM2 or this study. Model biases in simulated sea salt and high variability in mineral dust aerosol contribute to uncertainty and variability in model predicted INP populations. These biases were only modestly

influenced by changes to the coarse mode aerosol parameters, as described in Text S2 in Supporting Information S1. We note that the observation-based INP closure study (Section 4.1) suggests coarse mode aerosol does not significantly contribute to the observed aerosol surface area used in the M18 parameterization for marine INP prediction.

An important goal for representing SO INP populations and how they may change in response to climate change, including changes in transport patterns and land use change, is the ability to accurately attribute INPs to their sources. Over the SO region, marine and mineral dust INPs are likely the key INP types (C. H. Twohy et al., 2021). In this study, surface-level model-predicted INP populations were minimally influenced by simulated mineral dust aerosol estimated using D15, consistent with (Zhao et al., 2023). In contrast, N12-predicted mineral dust INPs resulted in an over-prediction of refractory INPs. The reported discrepancies between D15 and N12 are in contrast to reported agreements between N12 and D15 in dust events. While the D15 parameterization relates INPs to dust particles larger than 0.5 μm, the N12 parameterization relates dust INP to dust particles of any size. Additionally, mineral dust concentrations over the SO are far below the mineral dust aerosol amounts used to develop N12 and D15. These aerosol surface area or number concentration limits should be considered before using N12 and D15 in numerical modeling or INP closure studies.

While the M18 + D15 approach for predicting surface-level INP populations measured during MARCUS was largely successful, the skill in predicting INP populations above the ocean surface were highly variable. Poor skill in reproducing measured INP populations may be due to uncertainties in mineral dust aerosol and also in adequately representing marine aerosol at high latitudes. While back trajectories indicated that refractory INPs detected during MARCUS were sometimes associated with air masses originating from the Antarctic continental edge, additional observations of speciated aerosol mass concentrations, aerosol size number distributions, and INP composition are needed to further elucidate model errors in simulating SO aerosol, their associated INPs, and their impacts on Southern Ocean cloud properties.

Data Availability Statement

All SOCRATES observation data are available from the NCAR Earth Observation Lab (EOL) Field Catalog (http://catalog.eol.ucar.edu/socrates), including state and microphysics measurements (Laboratory, 2019b), aerosol composition (C. Twohy & Toohey, 2020), giant nuclei impactor (Laboratory, 2019a), and ice spectrometer data (P. DeMott & Hill, 2022). All MARCUS observation data are available from the DOE ARM archive at http://adc.arm.gov and the DOE ARM Intensive Operation Period (IOP) Data Browser, including nephelometer (Salwen et al., 2011) and ice spectrometer (P. J. DeMott, 2018) data. Model simulations are archived online (McCluskey, 2022).

References

Barry, K. R., Hill, T. C., Jentzsch, C., Moffett, B. F., Stratmann, F., & DeMott, P. J. (2021). Pragmatic protocols for working cleanly when measuring ice nucleating particles. *Atmospheric Research*, *250*, 105419. https://doi.org/10.1016/j.atmosres.2020.105419

Barry, K. R., Hill, T. C. J., Levin, E. J. T., Twohy, C. H., Moore, K. A., Weller, Z. D., et al. (2021b). Observations of ice nucleating particles in the free troposphere from Western US Wildfires. *Journal of Geophysical Research: Atmospheres*, *126*(3), e2020JD033752.. https://doi.org/10.1029/2020JD033752

Bigg, E. K. (1953). "The formation of atmospheric ice crystals by the freezing of droplets." *Quarterly Journal of the Royal Meteorological Society*, *79*(342), 510–519.

Bjordal, J., Storelvmo, T., Alterskjær, K., & Carlsen, T. (2020). Equilibrium climate sensitivity above 5°C plausible due to state-dependent cloud feedback. *Nature Geoscience*, *13*(11), 718–721. https://doi.org/10.1038/s41561-020-00649-1

Bodas-Salcedo, A., Hill, P. G., Furtado, K., Williams, K. D., Field, P. R., Manners, J. C., et al. (2016). Large contribution of supercooled liquid clouds to the solar radiation budget of the Southern Ocean. *Journal of Climate*, *29*(11), 4213–4228. https://doi.org/10.1175/JCLI-D-15-0564.1

Bogenschutz, P. A., Gettelman, A., Morrison, H., Larson, V. E., Craig, C., & Schanen, D. P. (2013). Higher-order turbulence closure and its impact on climate simulations in the Community Atmosphere Model. *Journal of Climate*, *26*(23), 9655–9676. https://doi.org/10.1175/JCLI-D-13-00075.1

Cornwell, G. C., Sultana, C. M., Prank, M., Cochran, R. E., Hill, T. C. J., Schill, G. P., et al. (2020). Ejection of dust from the ocean as a potential source of marine ice nucleating particles. *Journal of Geophysical Research: Atmospheres*, *125*(24), e2020JD033073. https://doi.org/10.1029/2020JD033073

DeMott, P., & Hill, T. (2022). NSF/NCAR GV HIAPER ice spectrometer data. Version 1.0 [Dataset]. UCAR/NCAR - Earth Observing Laboratory. https://doi.org/10.26023/TTHZ-474E-B211

DeMott, P. J. (2018). MARCUS ice nucleating particle measurements [Dataset]. U.S. Department of Energy Data Explorer. https://doi.org/10.5439/1638968

DeMott, P. J., Hill, T., & McFarquhar, G. (2018). Measurements of Aerosols, Radiation, and Clouds over the Southern Ocean (MARCUS) ice nucleating particle measurements field campaign report (p. 12).

DeMott, P. J., Hill, T. C. J., McCluskey, C. S., Prather, K. A., Collins, D. B., Sullivan, R. C., et al. (2016). Sea spray aerosol as a unique source of ice nucleating particles. *Proceedings of the National Academy of Sciences*, *113*(21), 5797–5803. https://doi.org/10.1073/pnas.1514034112

DeMott, P. J., Prenni, A. J., McMeeking, G. R., Sullivan, R. C., Petters, M. D., Tobo, Y., et al. (2015). Integrating laboratory and field data to quantify the immersion freezing ice nucleation activity of mineral dust particles. *Atmospheric Chemistry and Physics*, *15*(1), 393–409. https://doi.org/10.5194/acp-15-393-2015

Eidhammer, T., DeMott, P. J., Prenni, A. J., Petters, M. D., Twohy, C. H., Rogers, D. C., et al. (2010). Ice initiation by aerosol particles: Measured and predicted ice nuclei concentrations versus measured ice crystal concentrations in an orographic wave cloud. *Journal of the Atmospheric Sciences*, *67*(8), 2417–2436. https://doi.org/10.1175/2010JAS3266.1

Feingold, G., & Kreidenweis, S. (2000). Does cloud processing of aerosol enhance droplet concentrations? *Journal of Geophysical Research*, *105*(D19), 24351–24361. https://doi.org/10.1029/2000JD900369

Gettelman, A., Bardeen, C. G., McCluskey, C. S., Järvinen, E., Stith, J., Bretherton, C., et al. (2020). Simulating observations of Southern Ocean clouds and implications for climate. *Journal of Geophysical Research: Atmospheres*, *125*(21). https://doi.org/10.1029/2020JD032619

Gettelman, A., Hannay, C., Bacmeister, J. T., Neale, R. B., Pendergrass, A. G., Danabasoglu, G., et al. (2019). High climate sensitivity in the Community Earth System Model Version 2 (CESM2). *Geophysical Research Letters*, *46*(14), 8329–8337. https://doi.org/10.1029/2019GL083978

Gettelman, A., Mills, M. J., Kinnison, D. E., Garcia, R. R., Smith, A. K., Marsh, D. R., et al. (2019). The Whole Atmosphere Community Climate Model Version 6 (WACCM6). *Journal of Geophysical Research: Atmospheres*, *124*(23), 12380–12403. https://doi.org/10.1029/2019JD030943

Golaz, J.-C., Larson, V. E., & Cotton, W. R. (2002). A PDF-based model for boundary layer clouds. Part II: Model results. *Journal of the Atmospheric Sciences*, *59*(24), 3552–3571. https://doi.org/10.1175/1520-0469(2002)059⟨3552:APBMFB⟩2.0.CO;2

Huang, Y., Protat, A., Siems, S. T., & Manton, M. J. (2015). A-train observations of Maritime Midlatitude Storm-Track Cloud Systems: Comparing the Southern Ocean against the North Atlantic. *Journal of Climate*, *28*(5), 1920–1939. https://doi.org/10.1175/JCLI-D-14-00169.1

Humphries, R. S., Keywood, M. D., Gribben, S., McRobert, I. M., Ward, J. P., Selleck, P., et al. (2021). Southern Ocean latitudinal gradients of cloud condensation nuclei. *Atmospheric Chemistry and Physics*, *21*(16), 12757–12782. https://doi.org/10.5194/acp-21-12757-2021

Jensen, J. B., Beaton, S. P., Stith, J. L., Schwenz, K., Colón-Robles, M., Rauber, R. M., & Gras, J. (2020). The Giant Nucleus Impactor (GNI)—A system for the impaction and automated optical sizing of giant aerosol particles with emphasis on sea salt. Part I: Basic instrument and algorithms. *Journal of Atmospheric and Oceanic Technology*, *37*(9), 1551–1569. https://doi.org/10.1175/JTECH-D-19-0109.1

Kanji, Z. A., Ladino, L. A., Wex, H., Boose, Y., Burkert-Kohn, M., Cziczo, D. J., & Krämer, M. (2017). Overview of ice nucleating particles. *Meteorological Monographs*, *58*, 1.1–1.33. https://doi.org/10.1175/AMSMONOGRAPHS-D-16-0006.1

Kay, J. E., Bourdages, L., Miller, N. B., Morrison, A., Yettella, V., Chepfer, H., & Eaton, B. (2016). Evaluating and improving cloud phase in the Community Atmosphere Model version 5 using spaceborne lidar observations: CAM cloud phase evaluation with CALIPSO. *Journal of Geophysical Research: Atmospheres*, *121*(8), 4162–4176. https://doi.org/10.1002/2015JD024699

Kupc, A., Williamson, C., Wagner, N. L., Richardson, M., & Brock, C. A. (2018). Modification, calibration, and performance of the ultra-high sensitivity aerosol spectrometer for particle size distribution and volatility measurements during the Atmospheric Tomography Mission (ATom) airborne campaign. *Atmospheric Measurement Techniques*, *11*(1), 369–383. https://doi.org/10.5194/amt-11-369-2018

Laboratory, U.-E. O. (2019a). Giant Cloud Condensation Nuclei (CCN) impactor data. Version 1.0 [Dataset]. UCAR/NCAR - Earth Observing Laboratory. https://doi.org/10.26023/HN9Y-HEMX-3C0J

Laboratory, U.-E. O. (2019b). SOCRATES: Low rate (LRT - 1 sps) navigation, state parameter, and microphysics flight-level data. Version 1.3 [Dataset]. UCAR/NCAR - Earth Observing Laboratory. https://doi.org/10.5065/D6M32TM9

Larson, V. E., Golaz, J.-C., & Cotton, W. R. (2002). Small-scale and mesoscale variability in cloudy boundary layers: Joint probability density functions. *Journal of the Atmospheric Sciences*, *59*(24), 3519–3539. https://doi.org/10.1175/1520-0469(2002)059⟨3519:SSAMVI⟩2.0.CO;2

Li, L., Mahowald, N. M., Kok, J. F., Liu, X., Wu, M., Leung, D. M., et al. (2022). Importance of different parameterization changes for the updated dust cycle modeling in the Community Atmosphere Model (version 6.1). *Geoscientific Model Development*, *15*(22), 8181–8219. https://doi.org/10.5194/gmd-15-8181-2022

Listowski, C., & Lachlan-Cope, T. (2017). The microphysics of clouds over the Antarctic Peninsula – Part 2: Modelling aspects within Polar WRF. *Atmospheric Chemistry and Physics*, *17*(17), 10195–10221. https://doi.org/10.5194/acp-17-10195-2017

Liu, X., Ma, P.-L., Wang, H., Tilmes, S., Singh, B., Easter, R. C., et al. (2016). Description and evaluation of a new four-mode version of the Modal Aerosol Module (MAM4) within version 5.3 of the Community Atmosphere Model. *Geoscientific Model Development*, *9*(2), 505–522. https://doi.org/10.5194/gmd-9-505-2016

Mace, G. G., & Protat, A. (2018). Clouds over the Southern Ocean as observed from the R/V investigator during CAPRICORN. Part I: Cloud occurrence and phase partitioning. *Journal of Applied Meteorology and Climatology*, *57*(8), 1783–1803. https://doi.org/10.1175/JAMC-D-17-0194.1

Mårtensson, E. M., Nilsson, E. D., Leeuw, G. D., Cohen, L. H., & Hansson, H.-C. (2003). Laboratory simulations and parameterization of the primary marine aerosol production. *Journal of Geophysical Research*, *108*(D9). https://doi.org/10.1029/2002JD002263

McCluskey, C. S. (2022). Archived model output for "simulating observations of Southern Ocean clouds and implications for climate" [Dataset]. Zenodo. https://doi.org/10.5281/zenodo.6463951

McCluskey, C. S., DeMott, P. J., Ma, P., & Burrows, S. M. (2019). Numerical representations of marine ice-nucleating particles in remote marine environments evaluated against observations. *Geophysical Research Letters*, *46*(13), 7838–7847. https://doi.org/10.1029/2018GL081861

McCluskey, C. S., Hill, T. C. J., Humphries, R. S., Rauker, A. M., Moreau, S., Strutton, P. G., et al. (2018). Observations of ice nucleating particles over Southern Ocean waters. *Geophysical Research Letters*, *45*(21), 11989–11997. https://doi.org/10.1029/2018GL079981

McCluskey, C. S., Hill, T. C. J., Malfatti, F., Sultana, C. M., Lee, C., Santander, M. V., et al. (2017). A dynamic link between ice nucleating particles released in nascent sea spray aerosol and oceanic biological activity during two mesocosm experiments. *Journal of the Atmospheric Sciences*, *74*(1), 151–166. https://doi.org/10.1175/JAS-D-16-0087.1

McCluskey, C. S., Hill, T. C. J., Sultana, C. M., Laskina, O., Trueblood, J., Santander, M. V., et al. (2018). A mesocosm double feature: Insights into the chemical makeup of marine ice nucleating particles. *Journal of the Atmospheric Sciences*, *75*(7), 2405–2423. https://doi.org/10.1175/JAS-D-17-0155.1

McCluskey, C. S., Ovadnevaite, J., Rinaldi, M., Atkinson, J., Belosi, F., Ceburnis, D., et al. (2018). Marine and terrestrial organic ice-nucleating particles in pristine marine to continentally influenced Northeast Atlantic air masses. *Journal of Geophysical Research: Atmospheres*, *123*(11), 6196–6212. https://doi.org/10.1029/2017JD028033

McCoy, I. L., Bretherton, C. S., Wood, R., Twohy, C. H., Gettelman, A., Bardeen, C. G., & Toohey, D. W. (2021). Influences of recent particle formation on Southern Ocean aerosol variability and low cloud properties. *Journal of Geophysical Research: Atmospheres*, *126*(8), e2020JD033529. https://doi.org/10.1029/2020JD033529

McFarquhar, G. M., Bretherton, C. S., Marchand, R., Protat, A., DeMott, P. J., Alexander, S. P., et al. (2021). Observations of clouds, aerosols, precipitation, and surface radiation over the Southern Ocean: An overview of CAPRICORN, MARCUS, MICRE, and SOCRATES. *Bulletin of the American Meteorological Society*, *102*(4), E894–E928. https://doi.org/10.1175/BAMS-D-20-0132.1

Meyers, M. P., DeMott, P. J., & Cotton, W. R. (1992). New primary ice-nucleation parameterizations in an explicit cloud model. *Journal of Applied Meteorology and Climatology*, *31*(7), 708–721.

Monahan, E. C., & Muircheartaigh, I. (1980). Optimal power-law description of oceanic whitecap coverage dependence on wind speed. *Journal of Physical Oceanography*, *10*(12), 2094–2099. https://doi.org/10.1175/1520-0485(1980)010⟨2094:OPLDOO⟩2.0.CO;2

Monahan, E. C., Spiel, D. E., & Davidson, K. L. (1986). A model of marine aerosol generation via whitecaps and wave disruption. In E. C. Monahan & G. M. Niocaill (Eds.), *Oceanic whitecaps: And their role in air-sea exchange processes* (pp. 167–174). Springer Netherlands. https://doi.org/10.1007/978-94-009-4668-2_16

Morrison, H., & Gettelman, A. (2008). A new two-moment bulk stratiform cloud microphysics scheme in the Community Atmosphere Model, version 3 (CAM3). Part I: Description and numerical tests. *Journal of Climate*, *21*(15), 3642–3659. https://doi.org/10.1175/2008JCLI2105.1

Niemand, M., Möhler, O., Vogel, B., Vogel, H., Hoose, C., Connolly, P., et al. (2012). A particle-surface-area-based parameterization of immersion freezing on desert dust particles. *Journal of the Atmospheric Sciences*, *69*(10), 3077–3092. https://doi.org/10.1175/JAS-D-11-0249.1

Noone, K. J., Ogren, J. A., Heintzenberg, J., Charlson, R. J., & Covert, D. S. (1988). Design and calibration of a counterflow virtual impactor for sampling of atmospheric fog and cloud droplets. *Aerosol Science and Technology*, *8*(3), 235–244. https://doi.org/10.1080/02786828808959186

O'Dowd, C. D., Facchini, M. C., Cavalli, F., Ceburnis, D., Mircea, M., Decesari, S., et al. (2004). Biogenically driven organic contribution to marine aerosol. *Nature*, *431*(7009), 676–680. https://doi.org/10.1038/nature02959

Raatikainen, T., Prank, M., Ahola, J., Kokkola, H., Tonttila, J., & Romakkaniemi, S. (2022). The effect of marine ice-nucleating particles on mixed-phase clouds. *Atmospheric Chemistry and Physics*, *22*(6), 3763–3778. https://doi.org/10.5194/acp-22-3763-2022

Salwen, C., Uin, J., Senum, G., Springston, S., & Andrews, E. (2011). ARM: AOS dry nephelometer 1 minute averages [Dataset]. U.S. Department of Energy Data Explorer. https://doi.org/10.5439/1259232

Sanchez, K. J., Roberts, G. C., Saliba, G., Russell, L. M., Twohy, C., Reeves, J. M., et al. (2021). Measurement report: Cloud processes and the transport of biological emissions affect southern ocean particle and cloud condensation nuclei concentrations. *Atmospheric Chemistry and Physics*, *21*(5), 3427–3446. https://doi.org/10.5194/acp-21-3427-2021

Spurny, K. R., & Lodge, J. P. (1972). Collection efficiency tables for membrane filters used in the sampling and analysis of aerosols and hydrosols. 735. https://doi.org/10.5065/D6F769JJ

Strapp, J. W., Leaitch, W. R., & Liu, P. S. K. (1992). Hydrated and dried aerosol-size-distribution measurements from the particle measuring systems FSSP-300 probe and the deiced PCASP-100X probe. *Journal of Atmospheric and Oceanic Technology*, *9*(5), 548–555. https://doi.org/10.1175/1520-0426(1992)009⟨0548:HADASD⟩2.0.CO;2

Tan, I., Storelvmo, T., & Zelinka, M. D. (2016). Observational constraints on mixed-phase clouds imply higher climate sensitivity. *Science*, *352*(6282), 224–227. https://doi.org/10.1126/science.aad5300

Twohy, C., & Toohey, D. (2020). Single particle composition via STEM/EDS. Version 1.0 [Dataset]. UCAR/NCAR - Earth Observing Laboratory. https://doi.org/10.26023/55HP-PSEF-WC07

Twohy, C. H., DeMott, P. J., Russell, L. M., Toohey, D. W., Rainwater, B., Geiss, R., et al. (2021). Cloud-nucleating particles over the Southern Ocean in a changing climate. *Earth's Future*, *9*(3). https://doi.org/10.1029/2020EF001673

Uetake, J., Hill, T. C. J., Moore, K. A., DeMott, P. J., Protat, A., & Kreidenweis, S. M. (2020). Airborne bacteria confirm the pristine nature of the Southern Ocean boundary layer. *Proceedings of the National Academy of Sciences*, *117*(24), 13275–13282. https://doi.org/10.1073/pnas.2000134117

Vali, G. (1971). Quantitative evaluation of experimental results an the heterogeneous freezing nucleation of supercooled liquids. *Journal of the Atmospheric Sciences*, *28*(3), 402–409. https://doi.org/10.1175/1520-0469(1971)028⟨0402:QEOERA⟩2.0.CO;2

Vali, G., DeMott, P. J., Möhler, O., & Whale, T. F. (2015). Technical note: A proposal for ice nucleation terminology. *Atmospheric Chemistry and Physics*, *15*(18), 10263–10270. https://doi.org/10.5194/acp-15-10263-2015

Vergara-Temprado, J., Miltenberger, A. K., Furtado, K., Grosvenor, D. P., Shipway, B. J., Hill, A. A., et al. (2018). Strong control of Southern Ocean cloud reflectivity by ice-nucleating particles. *Proceedings of the National Academy of Sciences*, *115*(11), 2687–2692. https://doi.org/10.1073/pnas.1721627115

Vergara-Temprado, J., Murray, B. J., Wilson, T. W., O'Sullivan, D., Browse, J., Pringle, K. J., et al. (2017). Contribution of feldspar and marine organic aerosols to global ice nucleating particle concentrations. *Atmospheric Chemistry and Physics*, *17*(5), 3637–3658. https://doi.org/10.5194/acp-17-3637-2017

Vignon, E., Alexander, S. P., DeMott, P. J., Sotiropoulou, G., Gerber, F., Hill, T. C. J., et al. (2021). Challenging and improving the simulation of mid-level mixed-phase clouds over the high-latitude Southern Ocean. *Journal of Geophysical Research: Atmospheres*, *126*(7), e2020JD033490. https://doi.org/10.1029/2020JD033490

Wang, Y., Liu, X., Hoose, C., & Wang, B. (2014). Different contact angle distributions for heterogeneous ice nucleation in the Community Atmospheric Model version 5. *Atmospheric Chemistry and Physics*, *14*(19), 10411–10430. https://doi.org/10.5194/acp-14-10411-2014

Wu, M., Liu, X., Yang, K., Luo, T., Wang, Z., Wu, C., et al. (2019). Modeling dust in East Asia by CESM and sources of biases. *Journal of Geophysical Research: Atmospheres*, *124*(14), 8043–8064. https://doi.org/10.1029/2019JD030799

Zelinka, M. D., Myers, T. A., McCoy, D. T., Po-Chedley, S., Caldwell, P. M., Ceppi, P., et al. (2020). Causes of higher climate sensitivity in CMIP6 models. *Geophysical Research Letters*, *47*(1). https://doi.org/10.1029/2019GL085782

Zender, C. S., Bian, H., & Newman, D. (2003). Mineral Dust Entrainment and Deposition (DEAD) model: Description and 1990s dust climatology. *Journal of Geophysical Research*, *108*(D14), 4416. https://doi.org/10.1029/2002JD002775

Zhao, X., Liu, X., Burrows, S., DeMott, P. J., Diao, M., McFarquhar, G. M., et al. (2023). Important ice processes are missed by the Community Earth System Model in Southern Ocean mixed-phase clouds: Bridging SOCRATES observations to model developments. *Journal of Geophysical Research: Atmospheres*, *128*(4), e2022JD037513. https://doi.org/10.1029/2022JD037513

Zhao, X., Liu, X., Burrows, S. M., & Shi, Y. (2021). Effects of marine organic aerosols as sources of immersion-mode ice-nucleating particles on high-latitude mixed-phase clouds. *Atmospheric Chemistry and Physics*, *21*(4), 2305–2327. https://doi.org/10.5194/acp-21-2305-2021